OPEN

Constitutive Intracellular Na^+ Excess in Purkinje Cells Promotes Arrhythmogenesis at Lower Levels of Stress Than Ventricular Myocytes From Mice With Catecholaminergic Polymorphic Ventricular Tachycardia

B. Cicero Willis, MD, MSc*; Sandeep V. Pandit, PhD*; Daniela Ponce-Balbuena, PhD; Manuel Zarzoso, PhD; Guadalupe Guerrero-Serna, PhD; Bijay Limbu, MS; Makarand Deo, PhD; Emmanuel Camors, PhD; Rafael J. Ramirez, PhD; Sergey Mironov, PhD; Todd J. Herron, PhD; Héctor H. Valdivia, MD, PhD; José Jalife, MD

Background—In catecholaminergic polymorphic ventricular tachycardia (CPVT), cardiac Purkinje cells (PCs) appear more susceptible to Ca^{2+} dysfunction than ventricular myocytes (VMs). The underlying mechanisms remain unknown. Using a CPVT mouse ($RyR2^{R4496C+/Cx40eGFP}$), we tested whether PC intracellular Ca^{2+} ($[Ca^{2+}]_i$) dysregulation results from a constitutive $[Na^+]_i$ surplus relative to VMs.

Methods and Results—Simultaneous optical mapping of voltage and $[Ca^{2+}]_i$ in CPVT hearts showed that spontaneous Ca^{2+} release preceded pacing-induced triggered activity at subendocardial PCs. On simultaneous current-clamp and Ca^{2+} imaging, early and delayed afterdepolarizations trailed spontaneous Ca^{2+} release and were more frequent in CPVT PCs than CPVT VMs. As a result of increased activity of mutant ryanodine receptor type 2 channels, sarcoplasmic reticulum Ca^{2+} load, measured by caffeine-induced Ca^{2+} transients, was lower in CPVT VMs and PCs than respective controls, and sarcoplasmic reticulum fractional release was greater in both CPVT PCs and VMs than respective controls. $[Na^+]_i$ was higher in both control and CPVT PCs than VMs, whereas the density of the Na^+/Ca^{2+} exchanger current was not different between PCs and VMs. Computer simulations using a PC model predicted that the elevated $[Na^+]_i$ of PCs promoted delayed afterdepolarizations, which were always preceded by spontaneous Ca^{2+} release events from hyperactive ryanodine receptor type 2 channels. Increasing $[Na^+]_i$ monotonically increased delayed afterdepolarization frequency. Confocal imaging experiments showed that postpacing Ca^{2+} spark frequency was highest in intact CPVT PCs, but such differences were reversed on saponin-induced membrane permeabilization, indicating that differences in $[Na^+]_i$ played a central role.

Conclusions—In CPVT mice, the constitutive $[Na^+]_i$ excess of PCs promotes triggered activity and arrhythmogenesis at lower levels of stress than VMs. **(*Circulation*. 2016;133:2348-2359. DOI: 10.1161/CIRCULATIONAHA.116.021936.)**

Key Words: arrhythmias, cardiac ■ calcium ■ calcium signaling ■ sodium-calcium exchanger

Catecholaminergic polymorphic ventricular tachycardia (CPVT) is an inheritable, proarrhythmogenic syndrome that affects ≈1 in 10 000 children.[1] CPVT is characterized by adrenergically mediated bidirectional VT or polymorphic VT that may lead to sudden cardiac death in the absence of structural heart disease.[2] CPVT may be caused by mutations in genes coding calcium handling proteins, including the cardiac sarcoplasmic reticulum (SR) Ca^{2+} release (ryanodine receptor type 2 [RyR2]) channel (*RYR2*),[3] calsequestrin (*CASQ2*),[4] triadin (*TRDN*),[5] and calmodulin (*CaM*).[6] The focus of this article is *RYR2*. Arrhythmias produced by gain-of-function mutations in RyR2 are postulated to result from destabilization of the channel with increased diastolic SR Ca^{2+} leak in ventricular myocytes (VMs), leading to delayed afterdepolarizations (DADs) and triggered activity via the Na^+/Ca^{2+} exchanger (NCX) current.[7,8]

Clinical Perspective on p 2359

Using a knock-in mouse model with a point mutation in RyR2 ($RyR2^{R4496C}$), we and others have postulated that Purkinje cells (PCs), not VMs, are the major source of triggered arrhythmogenic activity, including biventricular tachycardia.[9–11] There

Received February 6, 2016; accepted May 3, 2016.

From University of Michigan, Ann Arbor (B.C.W., S.V.P., D.P.-B., M.Z., G.G.-S., R.J.R., S.M., T.J.H., H.H.V., J.J.); Norfolk State University, VA (B.L., M.D.); University of Tennessee Health Science Center, Memphis (E.C.); and Fundación Centro Nacional de Investigaciones Cardiovasculares, Madrid, Spain (J.J.).

*Drs Willis and Pandit contributed equally to this work.

The online-only Data Supplement is available with this article at http://circ.ahajournals.org/lookup/suppl/doi:10.1161/CIRCULATIONAHA.116.021936/-/DC1.

Correspondence to José Jalife, MD, Center for Arrhythmia Research, University of Michigan, 2800 Plymouth Rd, Ann Arbor, MI 48109. E-mail jjalife@umich.edu

is also evidence supporting a prominent role for the PC conducting system in triggered activity and arrhythmogenesis in the *CASQ2*$^{-/-}$ model of CPVT.[12] These findings have spawned increasing interest in the mechanisms of intracellular Ca^{2+} $[Ca^{2+}]_i$ homeostasis of the cardiac PCs in both diseased and healthy hearts. PCs have an increased incidence of early afterdepolarizations (EADs) and DADs compared with VMs.[13] PCs have greater sensitivity to arrhythmogenesis in conditions of Ca^{2+} overload, produced by agents such as digitalis compounds that block the membrane Na/K ATPase, perhaps in part as a result of reduced transcript abundance of that protein in PCs versus VMs.[14] PCs from CPVT mice have a shorter latency and a lower threshold to develop spontaneous Ca^{2+} release (SCR) events than VMs.[11] Whether this applies also to the whole heart and whether SCR triggers premature ventricular complexes that propagate from the Purkinje system to the ventricles remain to be determined. Most important, the question of what makes PCs more susceptible to arrhythmogenesis in CPVT than VMs has never been addressed. Answering the above questions may lead to novel and more effective antiarrhythmic therapeutic strategies in CPVT and other cardiac diseases associated with Ca^{2+}-linked ventricular arrhythmias.

Our main objective in this study was 2-fold: to test whether Ca^{2+} dysregulation from within the Purkinje network underlies focal triggered activity in CPVT hearts ($RyR2^{R4496C+/-}$) and to establish whether a higher $[Na^+]_i$ in mouse PCs than VMs exacerbates $[Ca^{2+}]_i$ dysregulation in CPVT and explains their increased susceptibility to EADs, DADs, and triggered activity compared with VMs.

Methods

Expanded versions of the Methods are presented in the online-only Data Supplement.

Animals

The study was approved by the University Committee on the Use and Care of Animals at the University of Michigan. $RyR2^{+/Cx40eGFP+/-}$ (hereafter control) and $RyR2^{R4496C+/Cx40eGFP}$ (hereafter CPVT) mice were used to enable visualization of the Purkinje network and isolated PCs via green fluorescent protein expression (Figure I in the online-only Data Supplement).[11]

Optical Mapping

Optical mapping of the subendocardium was conducted in Langendorff-perfused hearts with di-4-ANBDQPQ and rhod-2 AM dyes, a single charge-coupled device camera, and a custom-made LED system.[15] Lead I ECGs were acquired and digitized at 1 kHz.[16] The protocol included 4 groups: baseline sinus rhythm, high-frequency (12 Hz) pacing, adrenergic stimulation (3.6 mmol/L Ca^{2+}, 160 nmol/L isoproterenol), and high-frequency pacing plus adrenergic stimulation.

Isolation of PCs and VMs

PCs and VMs were dissociated as previously described.[11,17,18] For permeabilized membrane experiments, cells were kept in Ca^{2+} free stopping buffer. Cells were used for electrophysiological recording within 4 to 6 hours after isolation.

Immunohistochemistry

Immunofluorescence was examined with a Nikon Eclipse Ti inverted confocal microscope with a ×63/1.2-NA oil objective (Nikon Inc, Tokyo, Japan) at ambient temperature. Rabbit anti-$Ca_V1.2$ (Alomone, Jerusalem, Israel) and mouse anti-RyR2 (Iowa Hybridoma Core, University of Iowa) antibodies were used.

Simultaneous Action Potential and Ca^{2+} Transient Measurements

Cells were perfused with Tyrode's solution (37°C) and patched with 2- to 3-MΩ glass pipettes filled with intracellular solution at pH 7.2. Ca^{2+} signals were recorded with a whole-cell fluorescence photometry acquisition system (IonOptix). Fluorescent signals were synchronized to action potential (AP) recordings. Cells were stimulated at increasing frequencies (1, 3, 5 Hz) by current injection via patch pipette.

Ca^{2+} Transients and Ca^{2+} Sparks

Cells were incubated for 30 minutes in Tyrode's solution containing 10 µmol/L rhod-2 AM, washed with a fluorophore-free solution, and de-esterified for 15 minutes. Cells were then perfused with Tyrode's solution at 37° C. Measurements were acquired with a Nikon A1R confocal microscope in line scan mode. For Ca^{2+} transients, cells were field stimulated at 1, 3, and 5 Hz. For Ca^{2+} spark analysis, a 2-second line scan image window was selected 3 seconds after a steady-state Ca^{2+} transient had decreased to baseline level.

Permeabilized Cellular Ca^{2+} Spark Recordings

VMs and PCs were perfused with 50 nmol/L free Ca^{2+} internal solution plus saponin 0.005% for 1 minute for membrane permeabilization. Then, cells were perfused for 5 minutes with internal solution containing 2.5 µmol/L fluo-4 penta-K^+ (LifeTechnologies). Confocal line scan recordings (4-second duration) were obtained and analyzed within 10 minutes after dye loading as described above.

SR Ca^{2+} Load

Cells were loaded with rhod-2 (Life Technologies) as described above. Cells were perfused with 37°C Tyrode's solution containing 1 mmol/L Ca^{2+} and paced at 3 Hz for 10 seconds. One hundred milliseconds after pacing, cells were quickly perfused with Tyrode's solution containing caffeine (10 mmol/L). Ca^{2+} transient amplitude was a fraction of the caffeine-induced Ca^{2+} transient amplitude. Time to 50% decay was estimated from time at maximal caffeine-induced Ca^{2+} transient amplitude.

Na^+/Ca^{2+} Exchange Current

Cells were perfused with external solution containing nifedipine (10 µmol/L), ouabain (1 mmol/L), and niflumic acid (10 µmol/L). Free Ca^{2+} in the pipette solution was 205 nmol/L, Current was elicited with a descending-ascending voltage ramp from a holding potential of −75 mV. Na^+/Ca^{2+} exchange current (I_{NCX}) density was determined as the $NiCl_2$ (1 mmol/L)-sensitive current.

$[Na]_i$ Measurements

$[Na]_i$ was measured with SBFI-AM as previously described.[19]

Statistical Analyses

Data are presented as mean±SEM, and values of $P<0.05$ were considered significant. The unpaired Student *t* test, Fisher exact test, Mann-Whitney *U* test, or Kruskal-Wallis test with Dunn posttest were performed when appropriate to compare experimental groups. Statistical analysis was carried out with GraphPad Prism software (version 6.0).

Biophysical Model of Murine PC

The model described in Vaidyanathan et al[18] was modified to include cytosolic Ca^{2+} waves and late sodium current (I_{NaL}). Two-dimensional cytosolic Ca^{2+} diffusion was implemented to reproduce

the 2-component Ca^{2+} transients in canine PCs.[20] Details are given in the online-only Data Supplement (Tables I–V and Figures II–IV in the online-only Data Supplement).

Computer Simulations

$[Na^+]_i$ was increased by reducing the magnitude of Na^+-K^+ pump current (I_{NaK}) as summarized in Table III in the online-only Data Supplement on the basis of earlier work (but also see Limitations).[19,21] The functional effects of RyR2 mutations were implemented by lowering the threshold of SR Ca^{2+} release.[22] Isoproterenol effects were implemented by altering the maximum conductance of Ca^{2+} currents (I_{CaL} and I_{CaT}),[23,24] inward rectifier current (I_{k1}), and I_{NaK}.[25] Table IV in the online-only Data Supplement provides details.

Results

Subendocardial Origin of Postpacing Triggered Beats

Previously, we demonstrated that polymorphic VT in the CPVT mouse model is attributable to focal discharges at multiple locations within the specialized conduction system.[9] Here, we provide direct evidence of both the origin and the triggering mechanisms of such ectopic activity. Abnormal electric activity was elicited in 6 of 7 (85.7%) CPVT hearts and in 3 of 7 (42.8%) control hearts treated with Tyrode's solution containing high Ca^{2+} and isoproterenol after burst pacing. Figure 1A shows a representative volume-conducted ECG tracing from a CPVT heart before and after burst pacing. Rapid electric pacing in the presence of high Ca^{2+} and isoproterenol generated a series of ectopic beats immediately after pacing cessation. Each ectopic beat is identified by a number (1–9) in the red box in Figure 1A.

The precise origin for each of the 9 abnormal beats was identified in endocardial optical maps (Figure 1B), with earliest breakthrough points represented by white and magenta regions. These 9 beats were overlaid onto a high-resolution fluorescent image of the heart displaying green fluorescent protein–expressing Purkinje fibers. Initial breakthroughs colocalized with Purkinje fiber sites within the subendocardial conducting network (Figure 1C), suggesting that such fibers were the source of arrhythmogenic focal activity.

Spontaneous Ca^{2+} Release Precedes Triggered Activity in Subendocardial PCs of the CPVT Mouse

We then examined the temporal relationship between $[Ca^{2+}]_i$ release and membrane voltage (Vm) with respect to triggered activity in the subendocardium of CPVT mouse hearts. Hearts were loaded with the Ca^{2+} indicator dye rhod-2 AM and the voltage sensitive dye di-4-ANBDQPQ. In Figure 2A, simultaneous single pixel Ca^{2+} (red) and voltage (black) signals at a Purkinje fiber location (asterisk in Figure 2C) are displayed with paired ECG recordings (blue). Continuous rapid pacing (dotted line) in the presence of high Ca^{2+} and isoproterenol elicited a run of VT (box in Figure 2A). During VT, the sequence of Ca^{2+} and Vm activation signals was opposite sinus rhythm (before pacing). In Figure 2B, examples of 1 sinus discharge (left) and 1 VT discharge (right) emphasize that difference. During the abnormal beat, SCR preceded membrane depolarization, giving rise to a triggered discharge. In Figure 2C, the optical signals were analyzed beat by beat at high spatiotemporal resolution in endocardial Vm-Ca^{2+} difference maps. In sharp contrast with sinus and recovery beats, the Ca^{2+} transient preceded depolarization during each triggered discharge and the mean map.

Subcellular Distribution of the L-type Ca^{2+} Channel and RyR2 in Mouse PCs

The previously demonstrated presence of T tubules in mouse PCs[26] suggests that dyadic structures exist within these cells. Therefore, we assessed whether mouse PCs contain 2 key Ca^{2+}

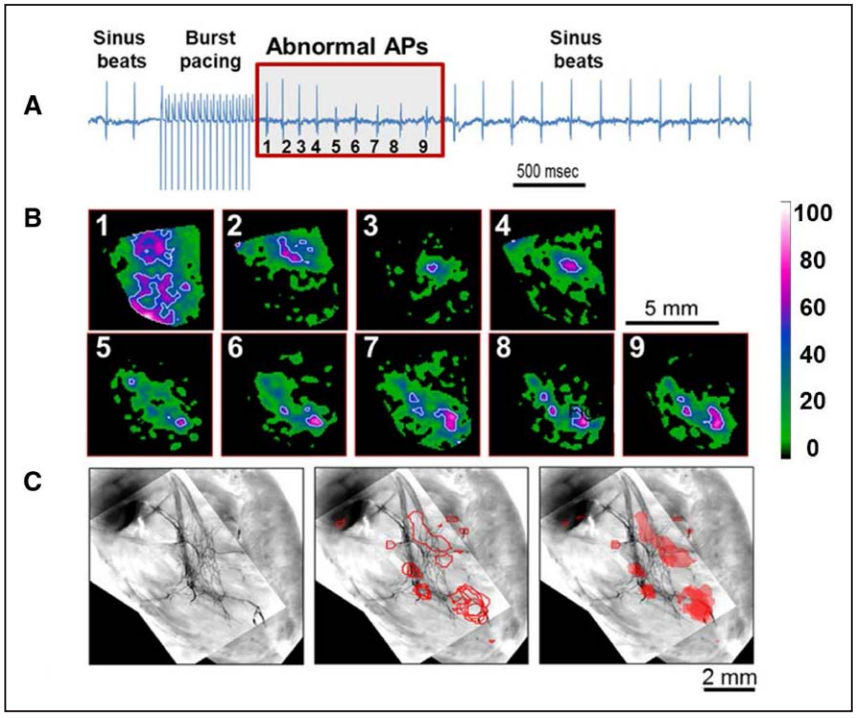

Figure 1. Subendocardial origins of spontaneous beats. **A**, Volume-conducted ECG recording of a catecholaminergic polymorphic ventricular tachycardia heart with 3.6 mmol/L Ca^{2+} and 160 nmol/L isoproterenol before, during, and after 12-Hz burst pacing. Nine abnormal action potentials (APs) were induced after pacing (red box, numbered). **B**, Earliest right ventricular endocardial AP wave breakthroughs of abnormal beats (1–9, each in a separate box) shown by white and magenta spots (color index bar represents percent from maximal signal in each frame). **C**, Image of green fluorescent protein–mapped area of the Purkinje network (**left**) superimposed with white contour lines from **B** (**middle** and **right**). Note colocalization of triggered beats with branches of the Purkinje conduction system.

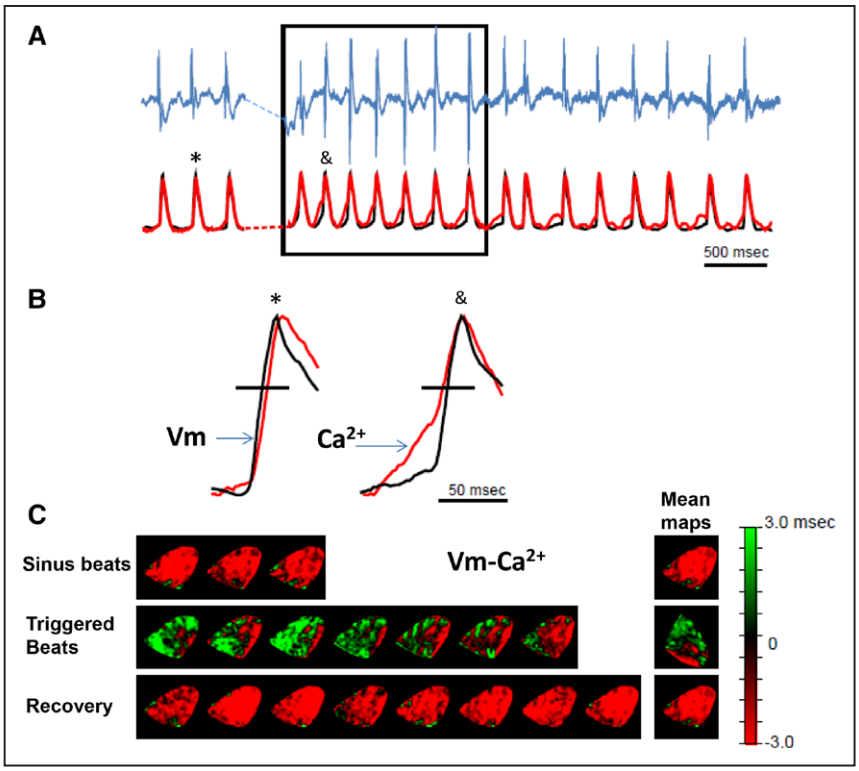

Figure 2. Spontaneous Ca^{2+} release precedes voltage depolarization during triggered activity in the subendocardium of the catecholaminergic polymorphic ventricular tachycardia heart. The heart was perfused with 3.6 mmol/L Ca^{2+} and 160 nmol/L isoproterenol. **A**, Volume-conducted ECG (**top**, blue) and optical signals obtained from a single pixel (black, voltage; red, Ca^{2+}) at the earliest breakthrough on a subendocardial Purkinje fiber location. **B**, Enlarged representative traces for sinus (**left**) and triggered (**right**) beats. Symbols on top identify the specific beats selected from **A**. **C**, Beat-to-beat (**left**) and mean (**right**) Vm-Ca^{2+} timing difference maps for sinus (**top**), triggered (**middle**), and recovery (**bottom**) beats measured at 60% maximum depolarization (horizontal black lines in **B**).

channels, L-type Ca^{2+} channel (α subunit, $Ca_V1.2$) and RyR2, in the dyad. Intracellular areas of RyR2 and $Ca_V1.2$ colocalizations were observed in both VMs and PCs isolated from control hearts; however, they were more heterogeneous in PCs than in VMs (Figure V in the online-only Data Supplement). Both proteins exhibited a striated staining pattern with significant colocalization at the sarcolemma (Figure Vb–Vd in the online-only Data Supplement) and at the expected T-tubule locations (Figure Ve and Vf in the online-only Data Supplement).

CPVT PCs Have a Lower Threshold for Triggered Activity Than VMs and Correlate With Abnormal Ca^{2+} Release

Figure 3 shows representative APs and Ca^{2+} transients recorded simultaneously from cells paced at 1 and 5 Hz in the absence and presence of isoproterenol. The addition of isoproterenol increased the Ca^{2+} transient amplitude in all cell types. Only CPVT VM and CPVT PC are shown because neither control VM nor control PC presented with abnormal beats during steady-state pacing (n=4 in each group). At steady-state baseline conditions (1-Hz pacing), no cells presented with abnormal Ca^{2+} handling or triggered activity, and each pacing-induced VM or PC AP was followed by a single Ca^{2+} transient (Figure 3A and 3B, left, paced beats indicated by black arrows). On addition of 30 nmol/L isoproterenol, only CPVT PCs exhibited triggered activity, mainly in the form of EADs (Figure 3A and 3B, right, abnormal beats indicated by blue arrows). At a faster pacing frequency (5 Hz), which leads to elevated SR Ca^{2+} load, CPVT PCs developed triggered activity even in the absence of isoproterenol (Figure 3D,

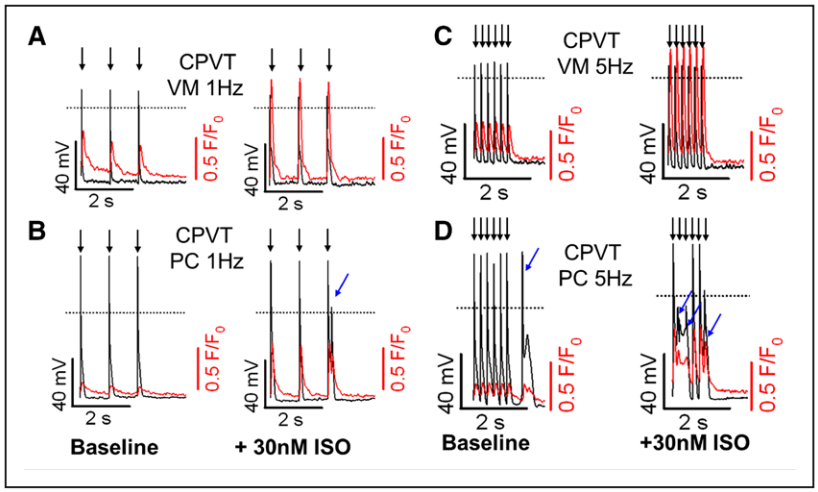

Figure 3. Catecholaminergic polymorphic ventricular tachycardia (CPVT) Purkinje cells (PCs) have lower threshold for Ca^{2+}-linked triggered activity. Representative simultaneous action potential (black) and Ca^{2+} fluorescence (red) recordings are presented on the same time scale. **A** and **B**, Steady-state 1-Hz pacing traces at baseline (**left**) and after 30 nmol/L isoproterenol (ISO) perfusion (**right**) for CPVT ventricular myocytes (VMs) and CPVT PCs, respectively. **C** and **D**, Steady-state 5-Hz pacing traces at baseline (**left**) and after 30 nmol/L isoproterenol perfusion (**right**) for CPVT VMs and CPVT PCs, respectively. Addition of isoproterenol significantly increases Ca^{2+} transient amplitude in both cell types. Neither control VMs nor control PCs developed abnormal beats under the same conditions (not shown). Black arrows indicate paced beats; blue arrows, spontaneous triggered activity.

left). In PCs paced at 5 Hz, spontaneous triggered activity and SCR increased significantly with 30 nmol/L isoproterenol (Figure 3D, right), which led to the appearance of both EADs and DADs coupled with early and late after Ca^{2+} transients. Altogether, CPVT PCs had shorter latencies and a higher incidence and number of events than CPVT VMs, as previously described.[9,11]

CPVT PCs Have a Higher Diastolic Ca^{2+} Leak

Three distinct patterns of SCR were observed in all cells: Ca^{2+} waves, early after- Ca^{2+} transients, and delayed after-Ca^{2+} transients (Figure VI in the online-only Data Supplement). As expected from previous reports showing a higher incidence of DADs, CPVT PCs had the highest incidence of SCR among the 4 cell types (Figure VII in the online-only Data Supplement).[9–11]

Representative baseline and post-isoproterenol Ca^{2+} spark 3-dimensional surface plots for CPVT VMs and PCs are shown in Figure 4A, demonstrating a larger number of Ca^{2+} sparks in CPVT PCs. In Figure 4B, quantification of Ca^{2+} spark recordings revealed that CPVT PCs had a significantly higher baseline Ca^{2+} spark frequency (CaSpF) after steady-state pacing compared with control VMs, control PCs, or CPVT VMs (10.4±2.4 versus 2.3±0.6, 4.4±0.9, and 4.4±1.3 sparks per 100 μm/s at 3 Hz, respectively; P=0.0002, P=0.0174, and P=0.0162). In Figure 4C, addition of isoproterenol (10 nmol/L) significantly and progressively increased CaSpF in all groups, with CPVT PCs having the highest CaSpF at all the time points recorded.

Decreased SR Ca^{2+} Load and Increased SR Fractional Release in CPVT

We next characterized the state of the SR Ca^{2+} load in CPVT PCs. Representative caffeine-induced Ca^{2+} transients after 3 Hz of steady-state pacing are illustrated in Figure 5A. In Figure 5B, the maximum amplitude of the caffeine-induced Ca^{2+} transient, an index of SR Ca^{2+} load, was significantly lower in each CPVT cell type compared with its control counterpart (CPVT VM versus control VM: $\Delta F/F_0$, 4.5±0.8 versus 8.6±1.7, P=0.0359; and CPVT PC versus control PCs: $\Delta F/F_0$, 2.7±0.4 versus 5.1±1.7, P=0.0416). Steady-state Ca^{2+} transient amplitude was presented as a fraction of the caffeine-induced Ca^{2+} transient amplitude, indicating fractional release. There was a significant increase in SR fractional release in both CPVT VM versus control VM (50.2±4.2% versus 31.2±3.0%; P=0.0011; Figure 5C) and CPVT PC versus control PC (59.2±11.3% versus 33.1±5.7%; P=0.0449), suggesting that Ca^{2+} gain was similarly altered by RyR2 gain of function in CPVT. Thus, the CPVT RyR2 mutation increased CaSpF, especially in PCs (Figure 4), despite a reduction in SR Ca^{2+} load.

Slower Cellular Ca^{2+} Extrusion in PCs Compared With VMs Is Attributable to Sarcolemmal Ionic Gradients

Time to 50% decay of the caffeine-induced Ca^{2+} transient, an indirect measure of NCX activity, was significantly prolonged in control PCs compared with control VMs (3.83±1.39 versus 1.51±0.12 seconds; P=0.0218; Figure 5D) and in CPVT PCs compared with CPVT VMs (3.46±1.61 versus 1.31±0.09 seconds; P=0.0359). There was no significant difference in this parameter between ventricular groups and between Purkinje groups. Whole-cell patch-clamp experiments revealed that I_{NCX} was similar in all 4 cell groups (I_{NCX} at 100 mV in control VMs, 1.7±0.4 pA/pF; CPVT VMs, 2.3±0.5 pA/pF; control PCs, 1.9±0.3 pA/pF; CPVT PCs, 2.0±0.2 pA/pF; P=0.9158; Figure 5E). Thus, although a slower caffeine-induced Ca^{2+} transient decay in control and CPTV PCs indicates that PCs have a reduced level of NCX functional expression than VMs, the voltage-clamp results failed to provide support for this idea. Both approaches measure function of NCX as opposed to Western blots or transcriptional levels of NCX. However,

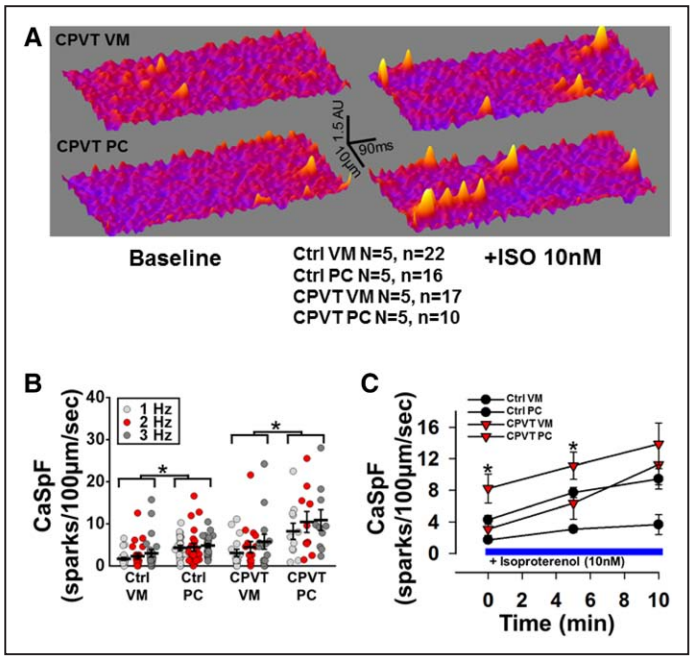

Figure 4. Ca^{2+} spark frequency (CaSpF) is higher in control and catecholaminergic polymorphic ventricular tachycardia (CPVT) Purkinje cells (PCs) than in ventricular myocytes (VMs). **A**, Three-dimensional surface plots of representative line scan images for a CPVT VM and CPVT PC for baseline (left) and 10 nM/L isoproterenol (right). **B**, Mean CaSpF at 1-, 3-, and 5-Hz stimulation. *P<0.05 vs control VMs at the same pacing frequency. #P<0.05 vs all other cell groups at the same pacing frequency. **C**, Time course of responses of CPVT VMs and CPVT PCs to isoproterenol (ISO; 10 nmol/L). *P<0.05 in Purkinje CPVT myocytes vs all other cell groups at same time point after isoproterenol.

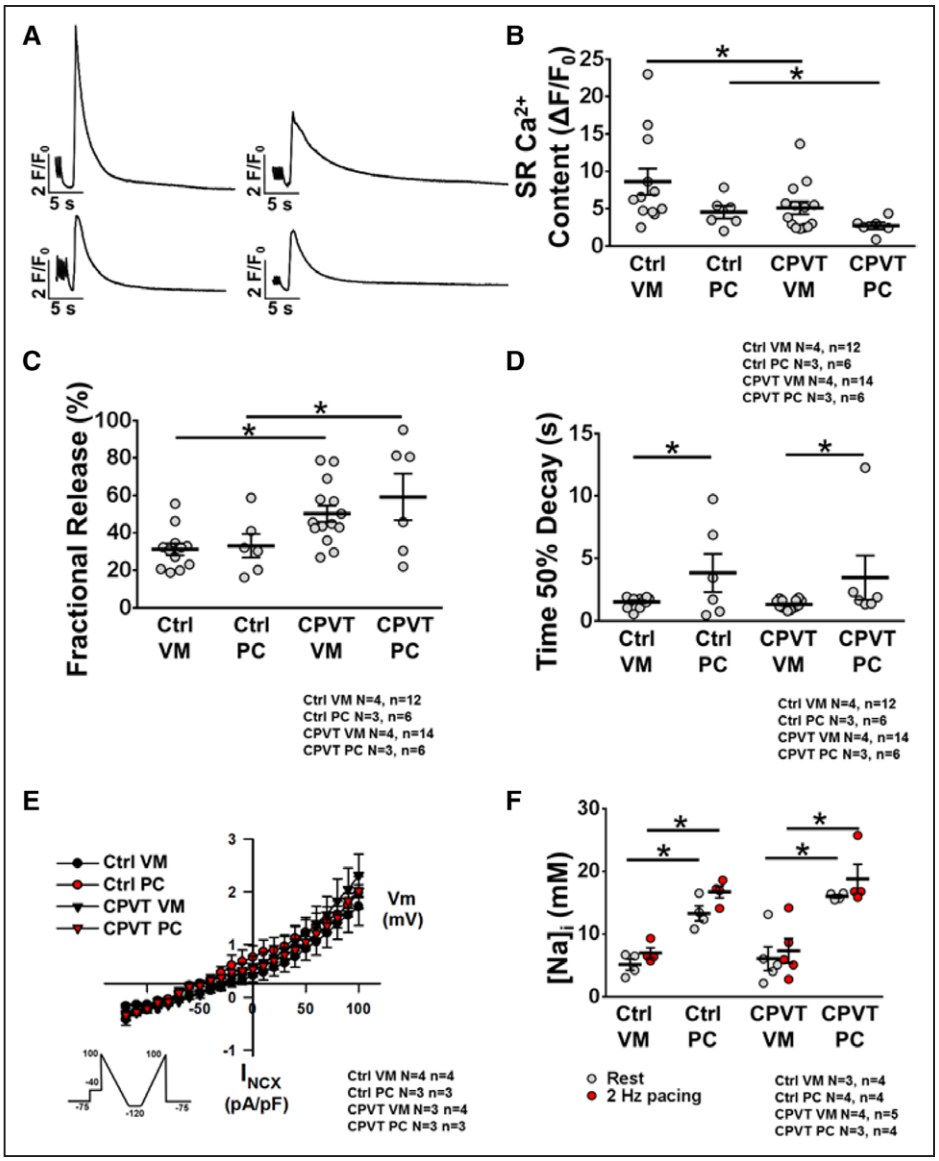

Figure 5. Sarcoplasmic reticulum (SR) Ca^{2+} handling and high $[Na^+]_i$ in Purkinje cells (PCs). **A**, Representative traces of caffeine-induced Ca^{2+} transient from control ventricular myocytes (VMs; **top left**) and PCs (**bottom left**) and catecholaminergic polymorphic ventricular tachycardia VMs (**top right**) and PCs (**bottom right**) recorded at 3-Hz stimulation with 10 mmol/L caffeine. **B**, Mean peak SR Ca^{2+} content in each cell type. **C**, SR fractional release and (**D**) time to 50% decay from caffeine-induced Ca^{2+} transient VMs. **E**, Average $NiCl_2$-sensitive Na^+/Ca^{2+} exchanger current/voltage relationships (voltage ramp protocol shown in the **inset**). **F**, Mean $[Na^+]$ concentration. *P<0.05.

the intracellular milieus at which the 2 functional assays measure NCX activity are vastly different from each other. One (caffeine-induced Ca^{2+} transient assay) is more physiological than the other.

Higher $[Na^+]_i$ in PCs at Rest and During Stimulation

$[Na^+]_i$ was measured in all 4 cellular groups at rest and after 2-Hz pacing. Figure 5F shows the average calibrated measurements for each group, and representative examples can be found in Figure VIII in the online-only Data Supplement. Control PCs compared with control VMs had significantly higher $[Na^+]_i$ at baseline (13.3±1.0 versus 5.2±0.8 mmol/L; P=0.0286) and under 2-Hz pacing (16.7±0.8 versus 7.0±0.7 mmol/L; P=0.0286). Likewise, CPVT PCs had significantly higher $[Na^+]_i$ both at baseline (16.0±0.2 versus 6.1±1.6 mmol/L; P=0.0159) and at 2-Hz pacing (18.8±2.0 versus 7.4±1.7 mmol/L; P=0.0159) compared with CPVT VMs. There were no differences in $[Na^+]_i$ between control VMs and CPVT VMs or between control PCs and CPVT PCs. Our calibrated $[Na]_i$ measurements with SBFI were conducted at physiological temperatures (37°C) and most likely underlie the reduced values of $[Na^+]_i$ in VMs (5–7 mmol/L) compared with the values shown by others in experiments conducted at room temperature, in the range of 11 to 15 mmol/L.[27] This is in line with the studies of Chapman[28] showing the relationship between intracellular Na activity and its sensitivity to temperature.

Higher $[Na^+]_i$ in PCs Increases SR Ca^{2+} Leak and Yields More Frequent DADs

To test the hypothesis that a constitutive excess in $[Na^+]_i$ in PCs promotes RyR2 leak and arrhythmias at lower levels of

stress than VMs, we conducted computer simulations in a well-tested model of the murine PC. The model accurately reproduces AP morphology, AP duration (APD) at 90% of repolarization (APD_{90}), and maximum dV/dt values obtained in experiments (Table II and Figure IV in the online-only Data Supplement).[18] Moreover, the model was able to reproduce the experimentally observed biphasic calcium transients resulting from both radial and longitudinal diffusion components (Figure IVC and IVD in the online-only Data Supplement).

In Figure 6A, the PC model with SCRs enabled was burst paced at 5 Hz for 10 seconds to overload the SR with calcium. At the end of pacing, a triggered AP was followed by a DAD, both of which were mediated via the cytosolic calcium waves. Similar to what happened in the experiments (Figure 3), simulating the effects of isoproterenol in the PC model significantly increased the frequency of SCR, thereby producing sustained DAD-induced triggered AP, as shown in Figure 6B. These results are in full agreement with our previously reported results in CPVT mice[9,11] and the experimental data presented above.

The $[Na^+]_i$ levels in the PC model were elevated by scaling I_{NaK} to 85%, 75%, and 65% of the control values (Table III in the online-only Data Supplement). Figure IXA and IXB in the online-only Data Supplement clearly shows that the APs were prolonged as a result of increased $[Na^+]_i$. Furthermore, the increased $[Na^+]_i$ was associated with elevated levels of averaged $[Ca^{2+}]$ in the model with progressively slower Ca^{2+} extrusion (Figure IXC in the online-only Data Supplement), which significantly increased the inward component of the NCX (Figure IXD in the online-only Data Supplement), leading to APD prolongation at higher $[Na^+]_i$. We did not observe noticeable changes in the resting membrane potential (Vrest) at elevated levels of $[Na]_i$ (Table VI in the online-only Data Supplement). Thus, the fast and slow inactivation gates, namely *h* and *j*, in the sodium current formulation did not change significantly (Figure X and Table VI in the online-only Data Supplement), indicating that the inactivation kinetics of sodium channels was not altered at the elevated $[Na]_i$ levels. We also investigated the effects of blocking I_{NaL} in our model. As listed in Table VII and shown in Figure XI in the online-only Data Supplement, blocking I_{NaL} abbreviated the APD (both APD_{50} and APD_{90}) at all levels of $[Na]_i$; however, dV/dtmax and Vrest were not altered significantly. When SCRs were implemented in these models of elevated $[Na^+]_i$, we observed frequent DADs (Figure 7A). The DADs were

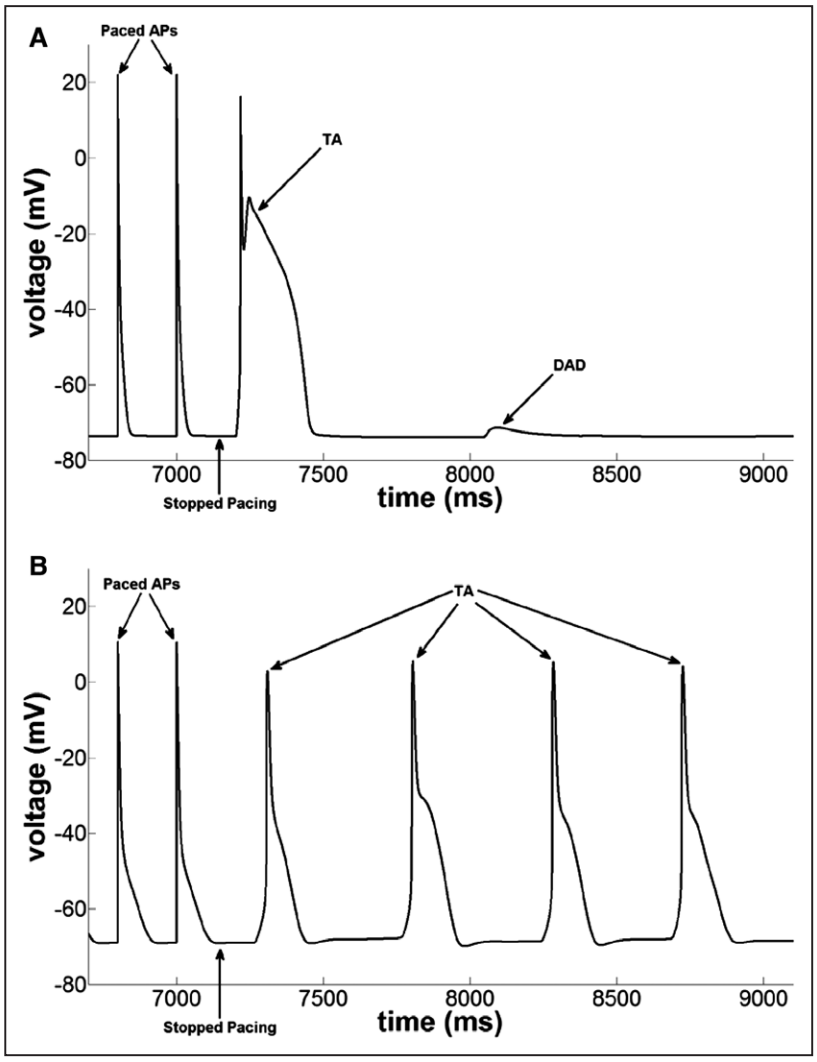

Figure 6. Pacing induced delayed afterdepolarizations (DADs) and triggered activity (TA) in the numeric mouse Purkinje cell model with spontaneous Ca^{2+} release enabled (catecholaminergic polymorphic ventricular tachycardia model; **A**) control case and (**B**) in the presence of isoproterenol effects followed by burst pacing at 5 Hz.

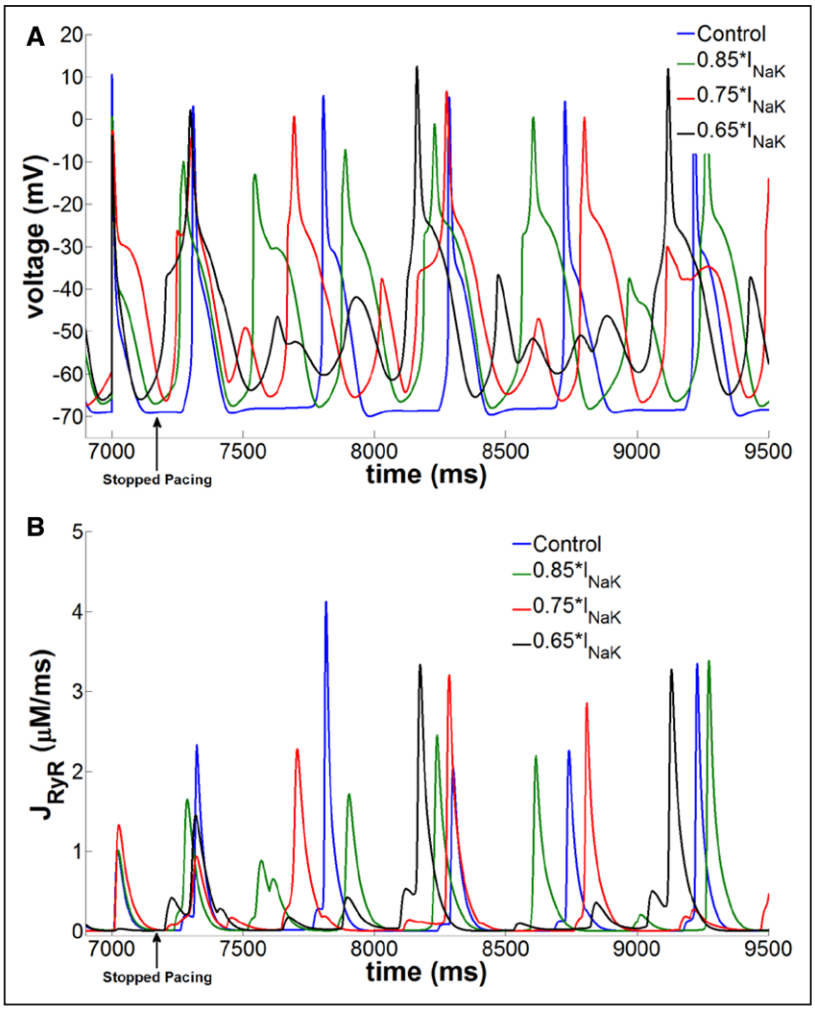

Figure 7. Ca^{2+}-linked arrhythmogenesis in the $[Na]_i$-overloaded numeric Purkinje cell model with isoproterenol effects. **A**, Generation of frequent delayed afterdepolarizations and triggered activity in the catecholaminergic polymorphic ventricular tachycardia model at various elevated levels of $[Na^+]_i$ obtained by reducing I_{NaK} density. **B**, Corresponding Ca^{2+} release flux from the ryanodine channels shows large-magnitude spontaneous Ca^{2+} release events preceding the membrane depolarizations.

always preceded by SCR events from the leaky RyR channels (Figure 7B). These RyR2 leaks initiated cytosolic Ca^{2+} waves, thus elevating the local Ca^{2+} concentration in the subsarcolemmal region. The elevated Ca^{2+} levels in the subsarcolemmal region activated the inward component of NCX, thereby producing DADs.

Membrane Permeabilization Reverses the Differential CaSpF in PCs Versus VMs

To provide further direct evidence that a higher $[Na]_i$ makes PCs more susceptible to RyR2 dysfunction than VMs, we measured Ca^{2+} sparks in saponin-permeabilized PCs and VMs. Figure 8A through 8D shows representative confocal line scan recordings of Ca^{2+} sparks in saponin-permeabilized control VMs, control PCs, CPVT VMs, and CPVT PCs with 50 nmol/L free Ca^{2+}. The CPVT mutation increased CaSpF significantly in CPVT VMs compared with control VMs (11.5±0.5 versus 5.8±0.5 sparks per 100 μm/s, respectively; $P<0.0001$; Figure 8E) and CPVT PCs to control PCs (8.0±0.7 versus 4.8±0.6 sparks per 100 μm/s, respectively; $P=0.0317$; Figure 8E). However, unlike intact cells (Figure 4), the CaSpF in control PCs was similar to that in control VMs (4.8±0.6 versus 5.8±0.5 sparks per 100 μm/s, respectively; $P=0.3087$; Figure 8E). Most important, CPVT PCs had lower CaSpF compared with CPVT VMs (8.0±0.7 versus 11.5±0.5 sparks per 100 μm/s, respectively; $P=0.0087$; Figure 8E).

Discussion

The major findings of this work may be summarized as follows. First, SCR preceded triggered activity in $RyR2^{R4496C+/-}$ CPVT hearts, whereas initial AP breakthrough points colocalized with the Purkinje conduction network, suggesting that PCs are the source of triggered activity in CPVT hearts. Second, in control and CPVT cardiomyocytes, CaSpF was greater in PCs than VMs at baseline and under β-adrenergic stress, reflecting increased activity of RyR2 channels. Third, CPVT mutation decreased SR Ca^{2+} load and increased fractional shortening in both PCs and VMs compared with control, suggesting that RyR2 Ca^{2+} sensitivity was equally increased by the CPVT mutation in PCs and VMs. Fourth, caffeine-induced Ca^{2+} transient decay was slower in control and CPVT PCs compared with VMs. Fifth, compared with VMs, both control and CPVT PCs had higher $[Na^+]_i$ at rest and during steady-state pacing. Sixth, in computer simulations, increasing $[Na^+]_i$ in a PC model cell greatly promoted RyR2 leak and arrhythmias. Finally, membrane permeabilization reversed the different PC versus VM postpacing CaSpF. Together, these results demonstrate for the first time the essential role of the constitutively

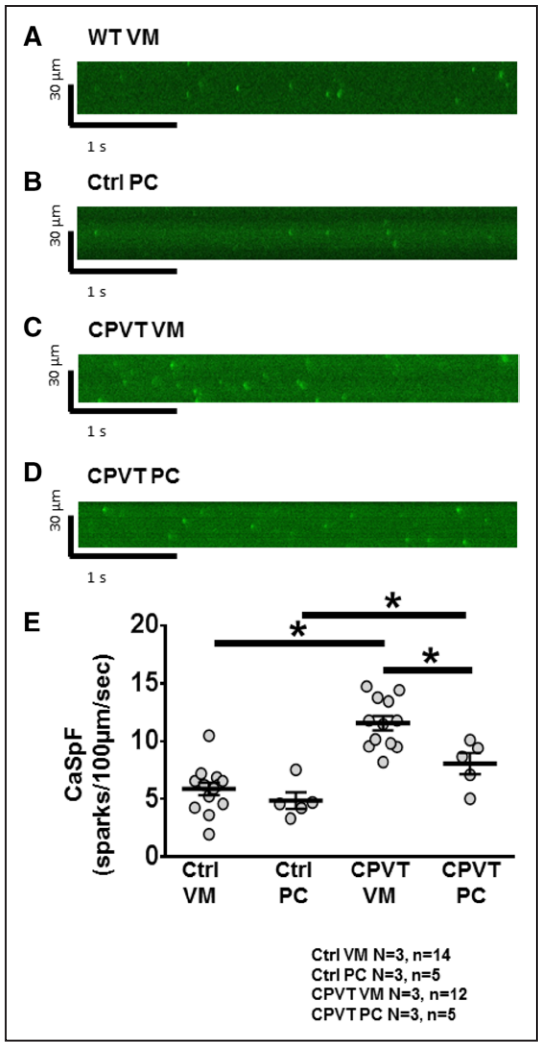

Figure 8. Membrane permeabilization terminates differential Ca^{2+} spark frequency (CaSpF) in Purkinje cells (PCs) compared with ventricular myocytes (VMs). **A** through **D**, Representative confocal line scan recordings showing Ca^{2+} sparks under 50 nmol/L free Ca^{2+} in permeabilized control VMs, control PCs, catecholaminergic polymorphic ventricular tachycardia (CPVT) VMs, and CPVT PCs. **E**, Average CaSpF among all groups. Note that there is no significant difference in CaSpF between control VMs and control PCs and that there is a significant decrease in CaSpF between CPVT VMs and CPVT PCs. *P<0.05.

higher PC $[Na^+]_i$ in promoting greater arrhythmogenicity than VMs in CPVT mice.

Subcellular Expression and Distribution of the L-type Ca^{2+} Channel and RyR2 Channels in Mouse PCs

The observation that (at least some) mouse PCs contain T tubules suggests the presence of normal dyadic structures that form at the sites of Ca^{2+} release at the junctional SR/T tubule membrane interfaces. Using fluorescent immunocytochemistry, we found that both control and CPVT mouse PCs express $Ca_V1.2$ and that this protein colocalizes with RyR2 to the same discrete subcellular locale, although with higher intercellular and intracellular heterogeneity than in VMs (Figure V in the online-only Data Supplement). These findings suggest that the main protein components of the classic Ca^{2+}-induced Ca^{2+} release process in VMs are present but are more heterogeneous in PCs.

Ca^{2+} Handling in Cardiac PCs

Although Ca^{2+} handling in VMs has been extensively studied and is relatively well understood, such is not the case for cardiac PCs. Previous studies have demonstrated that PCs are different from VMs, both morphologically and electrophysiologically.[9,18,29] We investigated whether inherent differences between the 2 cell types affect Ca^{2+} regulation and underlie the enhanced vulnerability of cardiac PCs over VMs to RyR2 dysfunction in CPVT. PCs are more arrhythmogenic than VMs in CPVT mice, and previous studies support the hypothesis that arrhythmias in the $RyR2^{R4496C+/-}$ mouse are caused by enhanced/abnormal diastolic Ca^{2+} release through defective RyR2 channels.[9,11] In this context, we sought to determine in the whole heart the role that cellular Ca^{2+} leak plays in $RyR2^{R4496C+/-}$ PCs. First, by measuring Vm and $[Ca^{2+}]_i$ simultaneously, we confirmed that PCs have a lower threshold for triggered activity, both during high-frequency pacing and under adrenergic stress (Figure 3). Most important, we determined that all DADs and EADs observed within mutant PCs correlated temporally with a synchronous rise in Ca^{2+}-mediated fluorescence. Then, to explore the mechanism for such findings, we dived further into the molecular basis of the Ca^{2+} handling machinery in mouse PCs.

Ca^{2+} sparks are stochastic activations of a cluster of RyR2s that form a Ca^{2+} release unit. In VMs, the synchronized opening of Ca^{2+} release units during Ca^{2+}-induced Ca^{2+} release is thought to generate a global Ca^{2+} transient in the cytosol. Although the Ca^{2+} release unit is incompletely understood in PCs, the general consensus is that in both VMs and PCs, Ca^{2+} sparks reflect cellular in situ activity of the RyR2. Therefore, it is well known that RyR2 Ca^{2+} sensitivity within Ca^{2+} release units correlates with a higher CaSpF. As shown in Figure 4, diastolic Ca^{2+} leak was higher in $RyR2^{R4496C+/-}$ mutant PCs compared with all other cell types, both at baseline and under β-adrenergic stress. To the best of our knowledge, this is the first time that Ca^{2+} sparks have been recorded in isolated murine PCs. An increased CaSpF resulting from increased RyR2 sensitivity is also in accordance with a decrease in SR Ca^{2+} load and an increase in SR fractional release, both of which were observed in CPVT PCs (Figure 5). Taken together, our results support the hypothesis that enhanced diastolic Ca^{2+} leak in PCs is responsible for triggered activity arising from the conduction system. Furthermore, we found that permeabilization of the membrane terminates this cell type–dependent difference in CaSpF (Figure 8). Together, these data suggest that a difference in the intracellular milieu that results from different transporters at the sarcolemmal membrane is an essential factor in making the PC more vulnerable to Ca^{2+} dysfunction than the VM.

What Is the Mechanism of the Increased Ca^{2+} Leak in the PCs?

We found that the caffeine-induced Ca^{2+} transient time to 50% decay was significantly prolonged in PCs. The caffeine transient decay time provides an indirect measure

of NCX-mediated cytosolic Ca^{2+} removal. Therefore, this would suggest that, at least after pacing, PCs in general have decreased activity of NCX compared with VMs. Through patch-clamp experiments, we determined that this is not attributable to decreased functional levels of NCX because I_{NCX} was not different among all 4 cell groups studied (Figure 5E). We postulate that the slower caffeine-induced Ca^{2+} transient decay time observed in control and CPVT PCs likely reflects changes in ionic gradients, particularly Na^+ gradients, which would slow NCX extrusion. Given that in the mouse heart PCs have a reduced density of T tubules[26] and larger I_{Na} density and are hyperpolarized compared with VMs,[18] it is reasonable to suggest that they are prone to Na^+ overload, which could also decrease postpacing NCX Ca^{2+} extrusion. We measured $[Na^+]_i$ and found that it was increased in PCs compared with VMs (Figure 5F), which is consistent with what has been shown in canine PCs.[30] Higher Na^+ load in PCs was also found in cells from CPVT hearts. These findings likely explain the increased caffeine-induced Ca^{2+} transient decay time observed in PCs compared with VMs because higher $[Na^+]_i$ would impair Ca^{2+} extrusion and lead to increased $[Ca^{2+}]_i$, as predicted by previous mathematical modeling[31] and by our own simulations (Figures 6 and 7). To the best of our knowledge, these results have not been reported previously in mouse PCs or in the context of inherited arrhythmogenic disease.

Intracellular Ca^{2+} Handling in Mouse PCs

PCs are different from VMs both morphologically and electrophysiologically.[10,11,18,32] In addition, $[Na^+]_i$ and Ca^{2+} homeostasis mechanisms are different in PCs and VMs.[33] In larger mammalian species, it has been shown that PCs have 2 types of SR, junctional and corbular,[34] and that this may underlie a Ca^{2+} activation process that is peculiar to the cell type and perhaps to the species.[35] For example, studies in canine PCs have shown that on electric stimulation there is an initial uniform Ca^{2+} rise under the cell membrane that propagates to the central core region via Ca^{2+}-induced Ca^{2+} release.[36,37] On the other hand, in CPVT, leaky RyR2 channels can initiate a Ca^{2+} wave that propagates from the core of a PC back to the membrane and causes depolarization. This reverse propagation of Ca^{2+} as a wave may then travel through the single PC, between cells, and along a fiber.[20]

On the basis of all the above, we propose that the constitutive excess of $[Na^+]_i$ in PCs with respect to VMs leads to PC $[Ca^{2+}]_i$ overload–induced SCR and triggered activity through an Na^+ overload–dependent decreased cytosolic Ca^{2+} extrusion mechanism. This potential mechanism becomes even more feasible when we consider that bidirectional VT has thus far been strongly associated only with CPVT and digitalis toxicity.[1,2,38,39] Indeed, the mechanism of action of digitalis is thought to be that of Na^+-dependent $[Ca^{2+}]_i$ overload through impaired NCX-mediated Ca^{2+} extrusion occurring as a consequence of Na^+/K^+ ATPase inhibition.[40] The functional density of Na^+/K^+ ATPase in the T tubules of VMs is 3- to 3.5-fold higher than in the lateral sarcolemma, and VMs have a ≈4- to 20-fold higher density of T tubules than PCs, depending on species, which may explain the higher conduction velocities in PC networks than VM.[21,26] Although the biophysical characterization of Na^+/K^+ ATPase in PCs is beyond the scope of this study, our measurements of $[Na^+]_I$, together with our computer simulations showing a strong dependence of SR Ca^{2+} leak on I_{NaK}, strongly support our conjecture that a PC $[Na^+]_i$ surplus drives calcium-linked ventricular arrhythmogenesis in mice. Nevertheless, further studies are warranted to elucidate the relationship between this important protein and triggered activity in PCs.

Limitations

We have not conducted direct measurements of $[Na^+]_i$ using Na^+-selective microelectrodes,[41] but our SFBI measurements were calibrated at the end of each experiment according to previous studies.[27] Some research groups have proposed a "triple layer" of Ca^{2+} activation in canine PCs involving IP3 receptors.[20] However, this mechanism may not hold true across different mammalian species. Although permeabilization of the cell membrane likely abolished the differences in $[Na^+]_i$ between PCs and VMs, at this point, we cannot exclude the possibility that the loss of an intracellular soluble factor contributed to the reversal of the different PC versus VM postpacing CaSpF. Obviously, although data on $[Na^+]_i$ differences in ventricular cells and Purkinje fibers obtained in mice and computer simulations can provide great insight into molecular and ionic mechanisms of inheritable cardiac diseases such as CPVT, extrapolation to other species and the human condition needs to be conducted with extreme caution. In our computer simulations, we have modeled elevated $[Na^+]_i$ on the basis of a reduced density of the I_{NaK} in PCs versus ventricular cells as in earlier studies.[31] However, whether differences in this current or those of other important regulators of $[Na^+]_i$ homeostasis such as the sodium-hydrogen exchanger and sodium-bicarbonate symporter[42] are important is unknown and will have to be investigated systematically in future studies. We have not accounted for alterations in both the hydrogen ion homeostasis and cell-coupling effects of the elevated Na values in PCs seen in our present study, which will need to be examined in the future. This is important because earlier studies have shown an important and complex relationship between changes in pH, $[Na^+]_i$, and rate of stimulation,[43] which may have implications for the generation of DADs.[44] Finally, unlike in other experimental models such as dogs,[45] mouse Purkinje fibers exhibit a similar density of the inward rectifier K^+ current (I_{K1}) in PCs and VMs, as shown in our earlier study.[19] Thus, I_{K1} does not play a role in the preferential formation of DADs in PCs compared with VMs, at least in mice, but this cannot be ruled out for other species, including humans.

Conclusions and Clinical Implications

CPVT is a congenital, proarrhythmogenic syndrome characterized by dangerous ventricular arrhythmias that appear under stress. CPVT has been linked to mutations in cardiac Ca^{2+} handling proteins, yet new evidence has shown that the cardiac Purkinje network appears to be involved in the initiation of bidirectional VT and PVT in this disease. This work has shed new light on the mechanisms of Ca^{2+}-linked ventricular arrhythmias arising from the cardiac Purkinje network in CPVT mice. Although translation from mouse model to humans is not trivial, our results present PC Na^+

and Ca^{2+} regulation as a new potential treatment avenue in CPVT and other cardiac diseases associated with Ca^{2+}-linked arrhythmias.

Acknowledgments

We thank Nulang Wang for her technical assistance.

Sources of Funding

This work was supported by National Heart, Lung, and Blood Institute grants P01-HL039707, P01-HL087226, and R01-HL122352; the Leducq Foundation: Transatlantic Network of Excellence Program on "Structural Alterations in the Myocardium and the Substrate for Cardiac Fibrillation" (Dr Jalife); grants HL055438 and HL120108 (to Dr Valdivia); and American Heart Association grant 12SDG11480010 (Dr Deo).

Disclosures

None.

References

1. Leenhardt A, Lucet V, Denjoy I, Grau F, Ngoc DD, Coumel P. Catecholaminergic polymorphic ventricular tachycardia in children: a 7-year follow-up of 21 patients. *Circulation*. 1995;91:1512–1519.
2. Venetucci L, Denegri M, Napolitano C, Priori SG. Inherited calcium channelopathies in the pathophysiology of arrhythmias. *Nat Rev Cardiol*. 2012;9:561–575. doi: 10.1038/nrcardio.2012.93.
3. Priori SG, Napolitano C, Tiso N, Memmi M, Vignati G, Bloise R, Sorrentino V, Danieli GA. Mutations in the cardiac ryanodine receptor gene (hRyR2) underlie catecholaminergic polymorphic ventricular tachycardia. *Circulation*. 2001;103:196–200.
4. Lahat H, Pras E, Olender T, Avidan N, Ben-Asher E, Man O, Levy-Nissenbaum E, Khoury A, Lorber A, Goldman B, Lancet D, Eldar M. A missense mutation in a highly conserved region of CASQ2 is associated with autosomal recessive catecholamine-induced polymorphic ventricular tachycardia in Bedouin families from Israel. *Am J Hum Genet*. 2001;69:1378–1384. doi: 10.1086/324565.
5. Roux-Buisson N, Cacheux M, Fourest-Lieuvin A, Fauconnier J, Brocard J, Denjoy I, Durand P, Guicheney P, Kyndt F, Leenhardt A, Le Marec H, Lucet V, Mabo P, Probst V, Monnier N, Ray PF, Santoni E, Trémeaux P, Lacampagne A, Fauré J, Lunardi J, Marty I. Absence of triadin, a protein of the calcium release complex, is responsible for cardiac arrhythmia with sudden death in human. *Hum Mol Genet*. 2012;21:2759–2767. doi: 10.1093/hmg/dds104.
6. Søndergaard MT, Sorensen AB, Skov LL, Kjaer-Sorensen K, Bauer MC, Nyegaard M, Linse S, Oxvig C, Overgaard MT. Calmodulin mutations causing catecholaminergic polymorphic ventricular tachycardia confer opposing functional and biophysical molecular changes. *FEBS J*. 2015;282:803–816. doi: 10.1111/febs.13184.
7. Liu N, Colombi B, Memmi M, Zissimopoulos S, Rizzi N, Negri S, Imbriani M, Napolitano C, Lai FA, Priori SG. Arrhythmogenesis in catecholaminergic polymorphic ventricular tachycardia: insights from a RyR2 R4496C knock-in mouse model. *Circ Res*. 2006;99:292–298. doi: 10.1161/01.RES.0000235869.50747.e1.
8. Faggioni M, Knollmann BC. Calsequestrin 2 and arrhythmias. *Am J Physiol Heart Circ Physiol*. 2012;302:H1250–H1260. doi: 10.1152/ajpheart.00779.2011.
9. Cerrone M, Noujaim SF, Tolkacheva EG, Talkachou A, O'Connell R, Berenfeld O, Anumonwo J, Pandit SV, Vikstrom K, Napolitano C, Priori SG, Jalife J. Arrhythmogenic mechanisms in a mouse model of catecholaminergic polymorphic ventricular tachycardia. *Circ Res*. 2007;101:1039–1048. doi: 10.1161/CIRCRESAHA.107.148064.
10. Kang G, Giovannone SF, Liu N, Liu FY, Zhang J, Priori SG, Fishman GI. Purkinje cells from RyR2 mutant mice are highly arrhythmogenic but responsive to targeted therapy. *Circ Res*. 2010;107:512–519. doi: 10.1161/CIRCRESAHA.110.221481.
11. Herron TJ, Milstein ML, Anumonwo J, Priori SG, Jalife J. Purkinje cell calcium dysregulation is the cellular mechanism that underlies catecholaminergic polymorphic ventricular tachycardia. *Heart Rhythm*. 2010;7:1122–1128. doi: 10.1016/j.hrthm.2010.06.010.
12. Mezu UL, Singh P, Shusterman V, Hwang HS, Knollmann BC, Němec J. Accelerated junctional rhythm and nonalternans repolarization lability precede ventricular tachycardia in Casq2-/- mice. *J Cardiovasc Electrophysiol*. 2012;23:1355–1363. doi: 10.1111/j.1540-8167.2012.02406.x.
13. Boyden PA, Hirose M, Dun W. Cardiac Purkinje cells. *Heart Rhythm*. 2010;7:127–135. doi: 10.1016/j.hrthm.2009.09.017.
14. Gaborit N, Le Bouter S, Szuts V, Varro A, Escande D, Nattel S, Demolombe S. Regional and tissue specific transcript signatures of ion channel genes in the non-diseased human heart. *J Physiol*. 2007;582(pt 2):675–693. doi: 10.1113/jphysiol.2006.126714.
15. Lee P, Klos M, Bollensdorff C, Hou L, Ewart P, Kamp TJ, Zhang J, Bizy A, Guerrero-Serna G, Kohl P, Jalife J, Herron TJ. Simultaneous voltage and calcium mapping of genetically purified human induced pluripotent stem cell-derived cardiac myocyte monolayers. *Circ Res*. 2012;110:1556–1563. doi: 10.1161/CIRCRESAHA.111.262535.
16. Noujaim SF, Pandit SV, Berenfeld O, Vikstrom K, Cerrone M, Mironov S, Zugermayr M, Lopatin AN, Jalife J. Up-regulation of the inward rectifier K+ current (I K1) in the mouse heart accelerates and stabilizes rotors. *J Physiol*. 2007;578(Pt 1):315–326. doi: 10.1113/jphysiol.2006.121475.
17. Anumonwo JM, Tallini YN, Vetter FJ, Jalife J. Action potential characteristics and arrhythmogenic properties of the cardiac conduction system of the murine heart. *Circ Res*. 2001;89:329–335.
18. Vaidyanathan R, O'Connell RP, Deo M, Milstein ML, Furspan P, Herron TJ, Pandit SV, Musa H, Berenfeld O, Jalife J, Anumonwo JM. The ionic bases of the action potential in isolated mouse cardiac Purkinje cell. *Heart Rhythm*. 2013;10:80–87. doi: 10.1016/j.hrthm.2012.10.002.
19. Despa S, Islam MA, Weber CR, Pogwizd SM, Bers DM. Intracellular Na(+) concentration is elevated in heart failure but Na/K pump function is unchanged. *Circulation*. 2002;105:2543–2548.
20. Stuyvers BD, Dun W, Matkovich S, Sorrentino V, Boyden PA, ter Keurs HE. Ca^{2+} sparks and waves in canine Purkinje cells: a triple layered system of Ca^{2+} activation. *Circ Res*. 2005;97:35–43. doi: 10.1161/01.RES.0000173375.26489.fe.
21. Despa S, Brette F, Orchard CH, Bers DM. Na/Ca exchange and Na/K-ATPase function are equally concentrated in transverse tubules of rat ventricular myocytes. *Biophys J*. 2003;85:3388–3396. doi: 10.1016/S0006-3495(03)74758-4.
22. Jiang D, Wang R, Xiao B, Kong H, Hunt DJ, Choi P, Zhang L, Chen SR. Enhanced store overload-induced Ca^{2+} release and channel sensitivity to luminal Ca^{2+} activation are common defects of RyR2 mutations linked to ventricular tachycardia and sudden death. *Circ Res*. 2005;97:1173–1181. doi: 10.1161/01.RES.0000192146.85173.4b.
23. Gaur N, Rudy Y, Hool L. Contributions of ion channel currents to ventricular action potential changes and induction of early afterdepolarizations during acute hypoxia. *Circ Res*. 2009;105:1196–1203. doi: 10.1161/CIRCRESAHA.109.202267.
24. Zhang LM, Wang Z, Nattel S. Effects of sustained beta-adrenergic stimulation on ionic currents of cultured adult guinea pig cardiomyocytes. *Am J Physiol Heart Circ Physiol*. 2002;282:H880–H889. doi: 10.1152/ajpheart.01138.2000.
25. Faber GM, Rudy Y. Calsequestrin mutation and catecholaminergic polymorphic ventricular tachycardia: a simulation study of cellular mechanism. *Cardiovasc Res*. 2007;75:79–88. doi: 10.1016/j.cardiores.2007.04.010.
26. Di Maio A, Ter Keurs HE, Franzini-Armstrong C. T-tubule profiles in Purkinje fibres of mammalian myocardium. *J Muscle Res Cell Motil*. 2007;28:115–121. doi: 10.1007/s10974-007-9109-6.
27. Despa S, Tucker AL, Bers DM. Phospholemman-mediated activation of Na/K-ATPase limits $[Na]_i$ and inotropic state during beta-adrenergic stimulation in mouse ventricular myocytes. *Circulation*. 2008;117:1849–1855. doi: 10.1161/CIRCULATIONAHA.107.754051.
28. Chapman RA. Sodium/calcium exchange and intracellular calcium buffering in ferret myocardium: an ion-sensitive micro-electrode study. *J Physiol*. 1986;373:163–179.
29. Cerrone M, Colombi B, Santoro M, di Barletta MR, Scelsi M, Villani L, Napolitano C, Priori SG. Bidirectional ventricular tachycardia and fibrillation elicited in a knock-in mouse model carrier of a mutation in the cardiac ryanodine receptor. *Circ Res*. 2005;96:e77–e82. doi: 10.1161/01.RES.0000169067.51055.72.
30. Lee CO, Dagostino M. Effect of strophanthidin on intracellular Na ion activity and twitch tension of constantly driven canine cardiac Purkinje fibers. *Biophys J*. 1982;40:185–198. doi: 10.1016/S0006-3495(82)84474-3.
31. Li P, Rudy Y. A model of canine Purkinje cell electrophysiology and Ca(2+) cycling: rate dependence, triggered activity, and comparison to ventricular myocytes. *Circ Res*. 2011;109:71–79. doi: 10.1161/CIRCRESAHA.111.246512.
32. Pallante BA, Giovannone S, Fang-Yu L, Zhang J, Liu N, Kang G, Dun W, Boyden PA, Fishman GI. Contactin-2 expression in the cardiac Purkinje

fiber network. *Circ Arrhythm Electrophysiol*. 2010;3:186–194. doi: 10.1161/CIRCEP.109.928820.
33. Vassalle M, Lin CI. Calcium overload and cardiac function. *J Biomed Sci*. 2004;11:542–565. doi: 10.1159/000079666.
34. Sommer JR, Johnson EA. Cardiac muscle: a comparative study of Purkinje fibers and ventricular fibers. *J Cell Biol*. 1968;36:497–526.
35. Rysevaite K, Saburkina I, Pauziene N, Vaitkevicius R, Noujaim SF, Jalife J, Pauza DH. Immunohistochemical characterization of the intrinsic cardiac neural plexus in whole-mount mouse heart preparations. *Heart Rhythm*. 2011;8:731–738. doi: 10.1016/j.hrthm.2011.01.013.
36. Bers DM. Cardiac excitation-contraction coupling. *Nature*. 2002;415:198–205. doi: 10.1038/415198a.
37. Boyden PA, Pu J, Pinto J, Keurs HE. Ca(2+) transients and Ca(2+) waves in Purkinje cells: role in action potential initiation. *Circ Res*. 2000;86:448–455.
38. Kummer JL, Nair R, Krishnan SC. Images in cardiovascular medicine. Bidirectional ventricular tachycardia caused by digitalis toxicity. *Circulation*. 2006;113:e156–e157. doi: 10.1161/CIRCULATIONAHA.105.557561.
39. Valent S, Kelly P. Images in clinical medicine: digoxin-induced bidirectional ventricular tachycardia. *N Engl J Med*. 1997;336:550. doi: 10.1056/NEJM199702203360805.
40. Hauptman PJ, Kelly RA. Digitalis. *Circulation*. 1999;99:1265–1270.
41. Shattock MJ, Bers DM. Rat vs. rabbit ventricle: Ca flux and intracellular Na assessed by ion-selective microelectrodes. *Am J Physiol*. 1989;256(pt 1):C813–C822.
42. Clancy CE, Chen-Izu Y, Bers DM, Belardinelli L, Boyden PA, Csernoch L, Despa S, Fermini B, Hool LC, Izu L, Kass RS, Lederer WJ, Louch WE, Maack C, Matiazzi A, Qu Z, Rajamani S, Rippinger CM, Sejersted OM, O'Rourke B, Weiss JN, Varró A, Zaza A. Deranged sodium to sudden death. *J Physiol*. 2015;593:1331–1345. doi: 10.1113/jphysiol.2014.281204.
43. Bountra C, Kaila K, Vaughan-Jones RD. Effect of repetitive activity upon intracellular pH, sodium and contraction in sheep cardiac Purkinje fibres. *J Physiol*. 1988;398:341–360.
44. Yano T, Hotokebuchi N, Morioka T, Nishi K. Acidosis depresses delayed afterdepolarization in guinea pig myocardium. *Am J Physiol*. 1989;257(pt 2):H996–1004.
45. Cordeiro JM, Zeina T, Goodrow R, Kaplan AD, Thomas LM, Nesterenko VV, Treat JA, Hawel L3rd, Byus C, Bett GC, Rasmusson RL, Panama BK. Regional variation of the inwardly rectifying potassium current in the canine heart and the contributions to differences in action potential repolarization. *J Mol Cell Cardiol*. 2015;84:52–60. doi: 10.1016/j.yjmcc.2015.04.010.

CLINICAL PERSPECTIVE

Catecholaminergic polymorphic ventricular tachycardia (CPVT) is a highly malignant, inheritable, proarrhythmogenic syndrome characterized by life-threatening ventricular arrhythmias that appear under stress. The work presented here sheds new light on the mechanisms of Ca^{2+}-linked ventricular arrhythmias in CPVT by demonstrating for the first time the essential role of the constitutively higher intracellular sodium of the specialized Purkinje cell in promoting greater arrhythmogenesis than ventricular myocytes in CPVT mice. CPVT has been linked to human mutations in cardiac Ca^{2+} handling proteins, yet new evidence has shown that the Purkinje network appears to be involved in the initiation of bidirectional and polymorphic ventricular arrhythmias in this disease. Although translation from the mouse model to the human should be done with caution, our results introduce the Purkinje cell Na^+ and Ca^{2+} regulation as a new potential target in CPVT and other cardiac diseases associated with Ca^{2+}-linked arrhythmias.

Constitutive Intracellular Na^+ Excess in Purkinje Cells Promotes Arrhythmogenesis at Lower Levels of Stress Than Ventricular Myocytes From Mice With Catecholaminergic Polymorphic Ventricular Tachycardia

B. Cicero Willis, Sandeep V. Pandit, Daniela Ponce-Balbuena, Manuel Zarzoso, Guadalupe Guerrero-Serna, Bijay Limbu, Makarand Deo, Emmanuel Camors, Rafael J. Ramirez, Sergey Mironov, Todd J. Herron, Héctor H. Valdivia and José Jalife

Circulation. 2016;133:2348-2359; originally published online May 11, 2016;
doi: 10.1161/CIRCULATIONAHA.116.021936
Circulation is published by the American Heart Association, 7272 Greenville Avenue, Dallas, TX 75231

Print ISSN: 0009-7322. Online ISSN: 1524-4539

Constitutive Intracellular Na^+ Excess in Purkinje Cells Promotes Arrhythmogenesis at Lower Levels of Stress than Ventricular Myocytes from Mice with Catecholaminergic Polymorphic Ventricular Tachycardia

B. Cicero Willis, MD; MSc,[1] Sandeep V. Pandit, PhD;[1] Daniela Ponce-Balbuena, PhD;[1] Manuel Zarzoso, PhD;[1] Guadalupe Guerrero-Serna, PhD;[1] Bijay Limbu, MS;[2] Makarand Deo, PhD;[2] Emmanuel Camors,[3] PhD; Rafael J. Ramirez, PhD;[1] Sergey Mironov, PhD; [1] Todd J. Herron, PhD;[1] Héctor H. Valdivia, MD, PhD;[1] José Jalife, MD.[1,4]

[1]University of Michigan, Ann Arbor, MI; [2]Norfolk State University, Norfolk, Virginia, [3]University of Tennessee Health Science Center. [4]Fundación Centro Nacional de Investigaciones Cardiovasculares (CNIC), Madrid, Spain.

Online Supplement

Experimental Methods

Animals: The study was approved by the University Committee on the Use and Care of Animals at the University of Michigan and conforms to the Guide for the Care and Use of Laboratory Animals (NIH publication no. 85-23). Procedures for the generation of $RyR2^{R4496C+/-}$ CPVT mice[1, 2], $Cx40^{eGFP+/-}$ mice[3], and $RyR2^{R4496C+/Cx40eGFP}$ mice[1, 4, 5] are described elsewhere. $RyR2^{+/Cx40eGFP+/-}$ (hereafter Ctrl) and $RyR2^{R4496C+/Cx40eGFP}$ (hereafter CPVT) mice were used to enable visualization of the Purkinje network and isolated PCs via GFP expression (Supplemental Fig. S1). All mice were of either sex and 3-6 months old.[5]

Optical mapping: Littermate Ctrl and CPVT mice were used for optical mapping experiments. In Langendorff-perfused hearts, optical mapping of the subendocardium was conducted using fluorescent voltage (di-4-ANBDQPQ) and Ca^{2+} indicator (rhod-2 AM) dyes. High-resolution optical mapping was performed using a single 80x80-pixel CCD camera (Sci Measure, Decatur, GA, USA) and a custom-made LED system consisting of three lights for variable excitation of each wavelength of interest (blue for GFP; red for di-4-ANBDQPQ; green for rhod-2 AM).[6] For endocardial imaging and mapping, the right ventricular free wall was dissected from apex to base. Care was taken to ensure that coronary artery perfusion was undisturbed, while still allowing exposure of the septal and free-wall endocardium. GFP images were taken of the

mapping area to identify the PC network architecture and provide an anatomical frame of reference for subsequent analyses. Images were taken at the start and completion of each experiment to ensure the preparation had not moved; and that optical mapping recordings could be overlaid on the images.

Hearts were cannulated and perfused with normal Tyrode's solution containing (in mM) 130.0 NaCl, 1.0 $MgCl_2$, 1.2 NaH_2PO_4, 4.0 KCl, 1.8 Ca^{2+}, 5.6 glucose and 25.0 HEPES, pH 7.4, bubbled with 95% O_2 5% CO_2. Lead-I volume-conducted ECGs were acquired and digitized at 1 kHz (Axon Instruments MiniDigi 1A digitizer and AxoScope 10 software).[7] Optical mapping movies (4-6 s) were recorded throughout the duration of each experiment. The experimental protocol included 4 condition/recording groups: 1) baseline sinus rhythm; 2) high-frequency (12 Hz) pacing; 3) adrenergic stimulation (3.6 mM Ca^{2+}, 160 nM ISO); and 4) high-frequency pacing plus adrenergic stimulation. Once sinus rhythm stabilized, we recorded a baseline GFP image, as well as simultaneous membrane voltage (Vm) and Ca^{2+} movies. We then began right ventricular (RV) free wall point stimulation at 12 Hz for ≈5 sec. Movies from the last second of pacing and subsequent 5 sec of unpaced activity were recorded. Similar Ca^{2+} and voltage recordings were taken 5 min after a bolus injection of ISO (160 nM) in the presence or the absence of 3.6 mM extracellular Ca^{2+}. Analysis was performed using custom-made software.[2, 6]

Isolation of PCs and VMs: Mouse cardiac PCs and VMs were dissociated as previously described.[5, 8, 9] Mice were euthanized by CO_2 overdose. The heart was quickly excised, placed in cardioplegic solution containing (in mmol/L): glucose 280, KCl 13.44, $NaHCO_3$ 12.6, and mannitol 34. The aorta was cannulated and retrogradely perfused at 37°C for 4 min with a Ca^{2+}-free perfusion buffer containing (in mmol/L): 113 NaCl, 4.7 KCl, 1.2 $MgSO_4$, 0.6 Na_2HPO_4, 0.6 KH_2PO_4, 10 $KHCO_3$, 12 $NaHCO_3$, 10 HEPES, 10 2.3-butanedione monoxime (BDM, Sigma), 30 taurine, and 5.5 glucose bubbled with 100% O_2. For enzymatic digestion, collagenase type II (Worthington; 773.4 u/ml), trypsin (0.14 mg/ml), and $CaCl_2$ (12.5 µmol/L) were added to the perfusion buffer for ~5 min. Following digestion the ventricles were cut open and Purkinje fibers were extracted from the subendocardial surfaces. Cells were isolated by trituration of the tissue suspension in stopping buffer (perfusion buffer plus 10% fetal bovine serum and 12.5 µmol/L $CaCl_2$). At 37^o C, the Ca^{2+} concentration was gradually increased to 1.0 mmol/L with ~5 min incubation steps. Cells were spun at 1000 rpm and re-suspended in Tyrode's solution containing (in mM): NaCl 148, KCl 5.4, $MgCl_2$ 1.0, $CaCl_2$ 1.0, NaH_2PO_4 0.4, glucose 5.5, HEPES 15, pH 7.4 (NaOH). For permeabilized membrane experiments, cells were kept in Ca^{2+} free stopping buffer. Cells were used for electrophysiological recording within 4-6 hours after isolation.

PC and VM immunohistochemistry: Isolated cells were plated on laminin-coated glass coverslips, fixed with 4% paraformaldehyde (10 min), permeabilized with 0.1% Triton X-100, and washed with PBS. Endogenous mouse immunoglobulin was blocked using a mouse-on-mouse (anti-mouse Ig) blocking reagent (M.O.M. kit; Vector Laboratories, Burlingame, CA, USA) for 1 h at room temperature. Cells were further blocked for 1 h with 5% normal donkey serum in PBS (containing 0.1% Triton X-100), and subsequently incubated with primary antibodies overnight at 4°C. After washing,

donkey secondary antibodies (anti-mouse and anti-rabbit) conjugated to DyLight fluorophores (488, 549 nm; Jackson ImmunoResearch Laboratories, West Grove, PA, USA) were added for 1 h. Nuclei were stained with 100 µM 4′-6-diamidino-2-phenylindole (DAPI) and washed, and coverslips were mounted to microscope slides using ProLong Gold Anti-Fade Mounting Kit (Molecular Probes, Eugene, OR, USA). Immunofluorescence was examined with a Nikon Eclipse Ti inverted confocal microscope with a ×63/1.2-NA oil objective (Nikon Inc., Tokyo, Japan) at ambient temperature. Rabbit anti-$Ca_V1.2$ (Alomone, Jerusalem, Israel) and mouse anti-RyR2 (Iowa Hybridoma Core, University of Iowa) antibodies were used.

Simultaneous action potential (AP) and Ca^{2+} transient measurements: APs were recorded with a MultiClamp 700B amplifier coupled to a Digidata 1440A digitizer (Molecular Devices). Isolated cells were patched using 2-3 MΩ borosilicate glass pipettes filled with intracellular solution containing (in mM): KCl 140.0, MgCl2 1.0, MgATP 7.0, NaGTP 0.3, HEPES 10.0 (pH 7.2 adjusted with KOH) with 100µM fluo-4 pentapotassium salt (Life Technologies). Isolated cells were placed on laminin coated corverslips and perfused with heated (37°C) Tyrode's solution. Ca^{2+} signals were recorded using a whole-cell fluorescence photometry acquisition system (IonOptix), with a 485±5 nm excitation light source emission filter and a 500-550 nm acquisition band pass filter. Fluorescent signals were synchronized to AP recordings via a TTL connection between systems. Single isolated VMs or PCs were selected within the fluorescence detection window, then gigaohm seal patch-clamped in the whole-cell configuration. Fluorescence gain and offset were appropriately adjusted. Cells were stimulated at increasing frequencies (1, 3, 5 Hz) by current injection via patch-pipette using a DS-8000 digital stimulator (World Precision Instruments) at twice threshold. Steady state and post-pacing baseline activities were recorded in all cells. Fluorescence analysis was performed using IonOptix software.

Ca^{2+} transients and Ca^{2+} sparks: Measurements were acquired with a Nikon A1R confocal microscope in line scan mode on a 12-bit (4096 grayscale) acquisition system. Pixel size was adjusted to 150 nm, pinhole aperture was 1.2 Airy units, and acquisition frequency was 512 Hz. Isolated cells were incubated for 30 min in normal Tyrode's solution containing 10 µM rhod-2 AM, then washed with a fluorophore-free solution and de-esterified for 15 min. Cells were placed on laminin-coated glass coverslips, mounted in a temperature-controlled superfusion chamber (37°C) and perfused with Tyrode's solution. Lines scans were parallel to the longitudinal axis of cells, avoiding cell nuclei. For Ca^{2+} transients, Ctrl and CPVT VMs and PCs were field-stimulated at incrementing pacing frequencies (1, 3, and 5 Hz) to reach steady-state SR Ca^{2+} load. The last paced event was recorded along with the subsequent 2-3 s for spontaneous Ca^{2+} spark recordings. The protocol was repeated at 1 Hz after 5 and 10 min of 10 nM ISO perfusion. Fluorescence data were normalized as $\Delta F/F_0$, where F is fluorescence intensity and F_0 is the average fluorescence at rest. For Ca^{2+} spark analysis, a 2-s line scan image window was selected 3 s after a steady-state Ca^{2+} transient had decreased to baseline level. Cells that developed Ca^{2+} waves within this time period were excluded from analysis. Ca^{2+} spark analysis was performed using ImageJ (National Institutes of Health).[10, 11]

Permeabilized cellular Ca^{2+} spark recordings: Isolated VM and PCs were perfused with 50nM free Ca^{2+} internal solution containing: (in mM): EGTA 0.5, HEPES 10, K-aspartate 120, $MgCl_2$ 0.56, $CaCl_2$ 0.12, ATP-Mg 5, reduced glutathione 10, phosphocreatine di-Na 5, creatine phosphokinase 5U/ml, dextran 4% plus saponin 0.005% for 1 min for membrane permeabilization, then perfused for 5 min with internal solution containing 2.5 μM fluo-4 penta-K^+ (LifeTechnologies). Confocal line scan recordings (4-s duration) were obtained and analyzed within 10 min after dye loading as described above.

SR Ca^{2+} load: Experiments were performed using the whole-cell fluorescence photometry acquisition system (IonOptix). Cells were loaded with rhod-2 (Life Technologies) as described above. Cells were placed on laminin-coated coverslips and perfused with heated (37°C) Tyrode's solution containing 1 mM Ca^{2+}. Single cells were electrically paced at 3Hz for 10 seconds to reach steady-state SR Ca^{2+} load. 100 ms after pacing, the cell was quickly perfused with Tyrode's solution containing caffeine (10mM). SR Ca^{2+} load was calculated from the $\Delta F/F_0$ of the cytosolic Ca^{2+} signal evoked by caffeine application. Steady-state Ca^{2+} transient amplitude was presented as a fraction of the caffeine induced Ca^{2+} transient amplitude. Time to 50% decay was estimated from time at maximal caffeine induced Ca^{2+} transient amplitude.

Na^+/Ca^{2+} exchange current (I_{NCX}): Whole cell patch-clamp recordings were performed using borosilicate glass pipettes (1.8-2.4 MΩ). Cells were perfused with external solution containing (in mM): 130 NaCl, 1.2 $MgSO_4$, 1.2 NaH_2PO_4, 1.8 $CaCl_2$, 10 HEPES, and 10 glucose (pH 7.4 with CsOH). Nifedipine (10 μM), ouabain (1 mM), and niflumic acid (10 μM) were added to block L-type Ca^{2+}, Na^+/K^+-ATPase and Cl^- currents, respectively. Pipette solution contained (in mM) 100 Cs^+-glutamate, 7.25 Na^+-HEPES, 1 $MgCl_2$, 12.75 HEPES, 2.5 Na_2ATP, 10 EGTA, and 6 $CaCl_2$ (pH 7.2 with CsOH). Free Ca^{2+} in pipette solution was 205 nM, calculated with dissociation constants given in MaxChelator software. Current was elicited using a descending-ascending voltage ramp (from +100 to -120 and back) from a holding potential of -75 mV. I_{NCX} density was determined as the $NiCl_2$ (1mM)-sensitive current, which was subtracted from baseline recordings and normalized to cell capacitance.

Intracellular Na^+ measurements ($[Na]_i$): Experiments were recorded and analyzed using a fluorescence photometry acquisition system (IonOptix). Briefly, isolated cells were incubated in Tyrode's solution containing 5μM SBFI-AM (Life Technologies) and 0.05% Pluronic F-127 for 2 hours, followed by 30 min in Tyrode's solution for desterification. Cells were plated in laminin-coated coverslips and perfused with warm (37°C) Tyrode's solution. Dual excitation (340 and 380 nm) was performed in each selected cell at rest and under 2Hz pacing (5 min). After pacing, each cell was perfused with divalent-free solution containing strophantidin (100μM) and gramicidin (10μM) and increasing free Na^+ concentrations (5, 10 and 20 mM Na^+, respectively), as previously described.[12] Background-subtracted F_{340}/F_{380} ratio was then converted to $[Na^+]_i$ by using a three-point calibration at the end of each experiment.

Biophysical numerical model of murine Purkinje cell: A morphologically realistic biophysical model of a murine cardiac Purkinje cell (PC) was developed starting from

the model of Vaidyanathan et al.[9] Figure S2 shows a schematic of the PC model. The cell is assumed to be cylindrical in shape with 129 µm length and 8 µm width which is within the experimentally measured dimensions of 129±7 µm and 8±0.3 µm, respectively.[9] Fig. S2B shows the intracellular compartmentalization of the model which is assumed to be symmetric along the length. The sarcolemmal (SL) currents are uniformly distributed along the length and the SR is assumed to be in the core of the cell. The membrane currents are collected in a subSL region of 0.5 µm depth immediately below the SL. The SR consists of two compartments: 1) a release compartment called Junctional SR (JSR) which is responsible for the release of Ca^{2+} from SR into the cytosol (blue arrow), and 2) an uptake compartment called Network SR (NSR) which is responsible for the uptake of Ca^{2+} from the cytosol into the SR (red arrow). Similar to SL, the ionic fluxes to and from the SR are collected in a sub-sarcoplasmic reticulum (subSR) region of 0.5 µm depth surrounding the SR. The radius of the SR is 4 µm and the total width of the cytosolic region is 2 µm surrounding the SR. The ionic formulations of the model were based on the work done by Li et al.[13] and modified according to the experimental data.[9] The ionic model described in [9] was modified to include late sodium current (I_{NaL}) as described in later section.

Cytosolic Ca^{2+} diffusion process: A realistic two component cytosolic Ca^{2+} diffusion process, as observed experimentally[14] was implemented in our model as follows: 1) Radial diffusion of Ca^{2+} entering the cell via SL Ca^{2+} channels (I_{CaL} and I_{CaT}) propagating towards central core (SR), referred to as wavelets, and 2) Cell wide longitudinal Ca^{2+} diffusion wave (CWW) initiated as a result of local CICRs propagating along the length of the cell. The length of the cell was divided into 10 discrete discs with each disc possessing L- and T-type SL Ca^{2+} channels and a SR compartment, whereas the width of the cell was divided into 81 concentric layers as shown in Fig. S3. The discretization of the cell volume was necessary to implement the uniform longitudinal and radial Ca^{2+} diffusion process. The number of SR discs was constrained to 10 to minimize the computational load while maintaining adequate spatiotemporal Ca^{2+} resolution.

A three dimensional diffusion equation was used to model the cytosolic Ca^{2+} diffusion process as follows:[15, 16]

$$\frac{\partial c}{\partial t} = \beta_i(c).[D_{Car}\frac{\partial^2 c}{\partial r^2} + \frac{D_{Car}}{r}\frac{\partial c}{\partial r} + D_{Cal}\frac{\partial^2 c}{\partial x^2} + J_{Ca}] \quad (1)$$

where c is the intracellular Ca^{2+} concentration, $D_{Car}\frac{\partial^2 c}{\partial r^2} + \frac{D_{Car}}{r}\frac{\partial c}{\partial r}$ term represents the radial diffusion and $D_{Cal}\frac{\partial^2 c}{\partial x^2}$ represents longitudinal diffusion. Here, D_{Cal} and D_{Car} represent the longitudinal and radial diffusion coefficients, respectively. J_{Ca} is the radially propagating Ca^{2+} flux from the SL channels and the ryanodine receptor flux from the SR and $\beta_i(c)$ represents the Ca^{2+} buffers. Finite Difference Time Domain (FDTD) solution[17] was used to a produce a finite and linear equivalent of Equation 1 as:

$$c_{(n,k,t)} = \beta_i(c_{(n,k,t)}) \frac{D_{Car}}{j_n(\Delta r)^2}[(1+j_n)c_{(n+1,k,t)} - 2j_n c_{(n,k,t)} + (j_n - 1)c_{(n-1,k,t)}] + \left\{ \frac{D_{Cal}}{(\Delta x)^2}[c_{(n,k+1,t)} - 2c_{(n,k,t)} + c_{(n,k-1,t)}] \right\} \quad (2)$$

Where $c_{(n,k,t)}$ represents intracellular Ca^{2+} concentration at a discrete node (n,k) at a time instance t. Here *n* represents the number of rows used in the model, *k* represents the number of columns used in the model, *Δr* is a small increment in width of model, *Δz* is a small increment in the length of the model, and j_n represents the n^{th} row along radial axis of cylindrical model. The value of the diffusion coefficient ($D_{Cal} = D_{Car} = D_{Ca}$) in our model was chosen to be 7 μm²/ms to reproduce experimentally observed Ca^{2+} transients. The Ca^{2+} transients obtained in our model are compared with the experimentally recorded values in Table S1.

Late sodium current (I_{NaL}): I_{NaL} formulation described in Li and Rudy[18] was included in the PC model. It included two components, namely, $I_{NaL,2}$ which peaks at -20 mV and $I_{NaL,3}$ which activates in the pacemaker range (see Equation 3

$$I_{NaL,2} = \overline{G}_{NaL,2} \cdot m_{L2} \cdot h_{L2} \cdot j_{L2} \cdot (V - E_{Na})$$
$$I_{NaL,3} = \overline{G}_{NaL,3} \cdot m_{L3} \cdot h_{L3} \cdot j_{L3} \cdot (V - E_{Na}) \quad (3)$$
$$I_{NaL} = I_{NaL,2} + I_{NaL,3}$$

where $\overline{G}_{NaL,x}$, m_{Lx}, h_{Lx}, and j_{Lx} are the maximum conductance, activation gate, fast inactivation gate, and slow inactivation gate of $I_{NaL,x}$ current, respectively. Further details about the gating parameters and initial conditions can be found in Ref. [9] The peak current density was adjusted to 1 pA/pF based on the experimental data reported by Iyer et al.[19] in mouse PCs.

The model was paced at 1 Hz for 5 mins to attain the steady state values. Table S2 provides a comparison of AP parameters obtained in our model with those of Vaidyanathan et al.[9] Fig. S3 shows the AP morphology of our model compared to the experimentally recoded AP.[9] Intracellular sodium concentration ($[Na^+]_i$) was increased by systematically reducing the sodium potassium pump current (I_{NaK}) as given in Table S3. Elevated $[Na^+]_i$ levels led to increase in the averaged intracellular Ca^{2+} in PC model as listed in Table S5.

Supplemental Tables

Table S1. The parameters of average calcium transients recorded in the experiments[1] and those obtained in the model.

Parameter	Experiments	Model
Peak Amplitude	31.193 ± 0.91 AU	1.03 µM
Time to Peak	18.8 ± 13.2 ms	27 ms
Decay time	261 ± 69.18 ms	199 ms

Table S2. Comparison of the AP parameters recorded in experiments[1] with those obtained in the model.

Parameter	Experiments	Model
dV/dtmax (mV/ms)	212±15	211.37
APD_{50} (ms)	4.7±0.3	7.7
APD_{70} (ms)	14.4±1.6	15.5
APD_{90} (ms)	68.6±5	67.1

Table S3. Intracellular sodium concentrations obtained for different scaling of I_{NaK}.

I_{NaK} scaling (%)	$[Na^+]_i$ (mM)
100 (Control)	12.42
85	13.57
75	14.58
65	15.91

Table S4. Modifications to the PC model for implementing the functional effects of isoproterenol.

Ionic Currents	Modification in percentage
I_{CaT}	230 %
I_{CaL}	140 %
I_{NaK}	170 %
I_{K1}	80 %

Table S5. Intracellular averaged calcium concentrations for different scaling of I_{NaK}.

I_{NaK} (%)	Peak Average $[Ca^{2+}]i$ (μM)
100 (Control)	1.03
85	1.28
75	1.49
65	1.81

Table S6. Resting membrane potentials and corresponding values of fast and slow inactivation gates (*h* and *j*, respectively) of I_{Na} at various elevated levels of $[Na]_i$.

I_{NaK} (%)	V_m (mV)	*h*	*j*
100 (Control)	-73.8	0.8384	0.8598
85	-73.6	0.8329	0.8541
75	-73.45	0.8282	0.8492
65	-73.27	0.8217	0.8423

Table S7. Action Potential characteristics in the PC model with and without I_{NaL}

I_{NaK} (%)	dV/dtmax (mV/ms)		Vrest (mV)		APD_{90} (ms)	
	With I_{NaL}	Without I_{NaL}	With I_{NaL}	Without I_{NaL}	With I_{NaL}	Without I_{NaL}
100 (Control)	211.37	212.2	-73.8	-73.95	67.1	51.4
85	206.72	207.73	-73.6	-73.75	78.3	59.9
75	202.73	203.9	-73.45	-73.65	85.4	64.8
65	197.54	199.05	-73.27	-73.45	95.5	71.5

Supplemental Figures

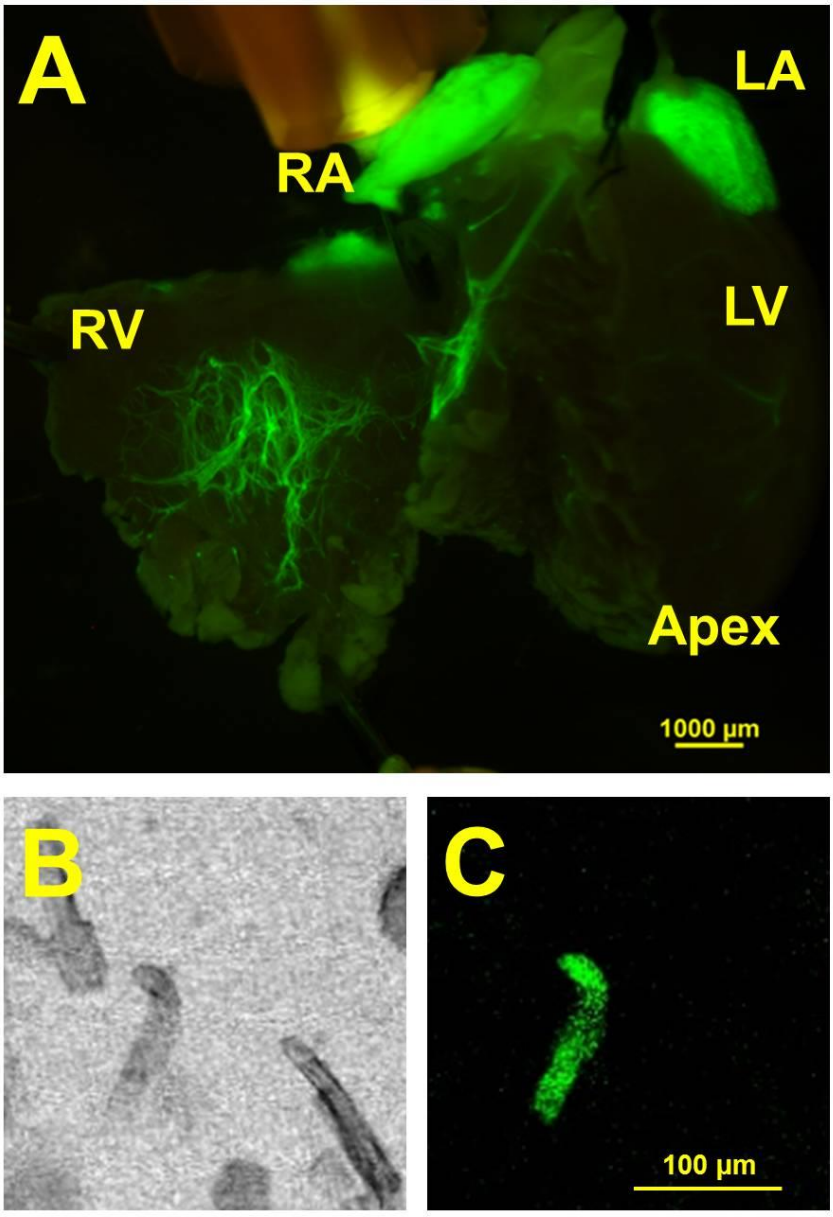

Supplement Fig. S1. Fluorescence of Cx40$^{eGFP+/-}$ mice endocardial Purkinje fibers and isolated PCs. (A) GFP fluorescence image of Cx40$^{eGFP+/-}$ CPVT heart RV endocardial preparation. (B) Light-transmitted and (C) fluorescence image of isolated GFP positive PC. LA= left atrium. LV= left ventricle. RA= right atrium. RV= right ventricle.

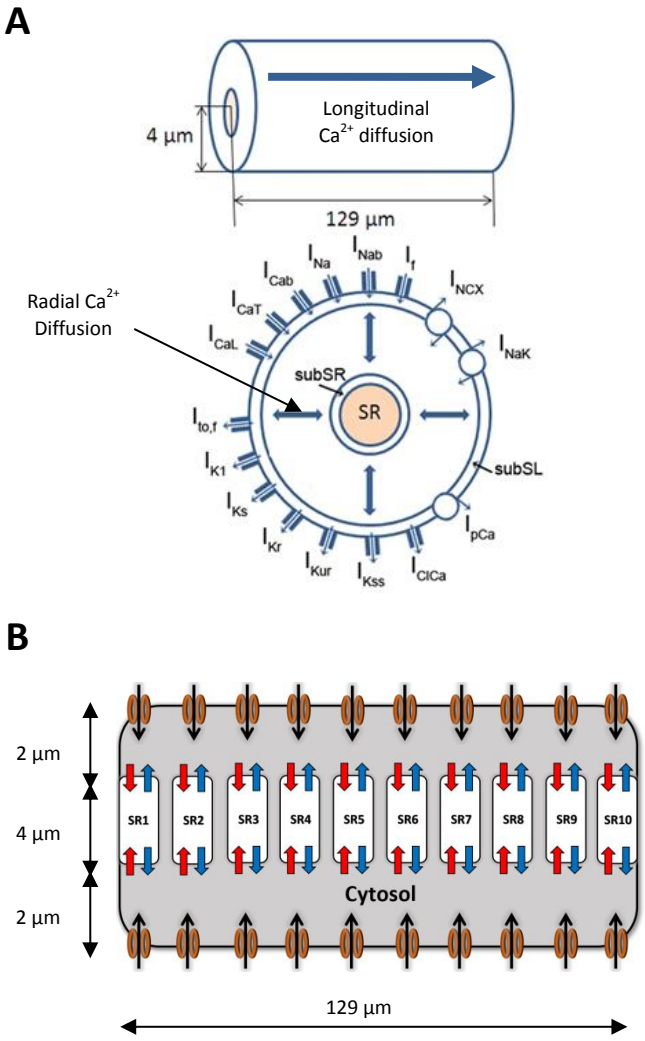

Supplemental Fig. S2. (A) Schematic showing various ionic currents and two components of Ca^{2+} diffusion (radial and longitudinal) in the PC biophysical model. (B) The sarcoplasmic reticulum (SR) is divided into 10 discrete sub compartments (SR1-SR10) along the cell length each having its own Ca^{2+} release/uptake machinery.

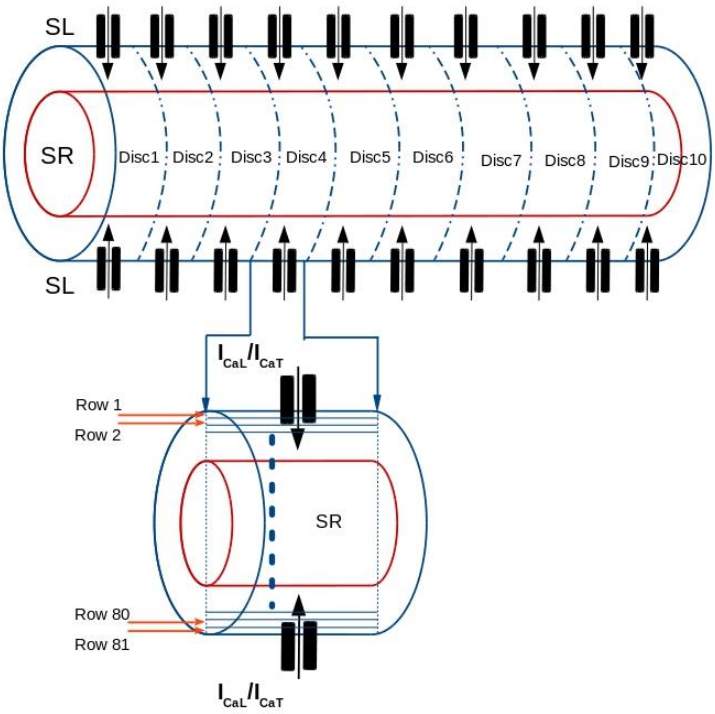

Supplemental Fig. S3. Implementation of spatio-temporal diffusion in the PC model. The Cell is divided into 10 Discs, each consisting of 81 concentric layers (rows).

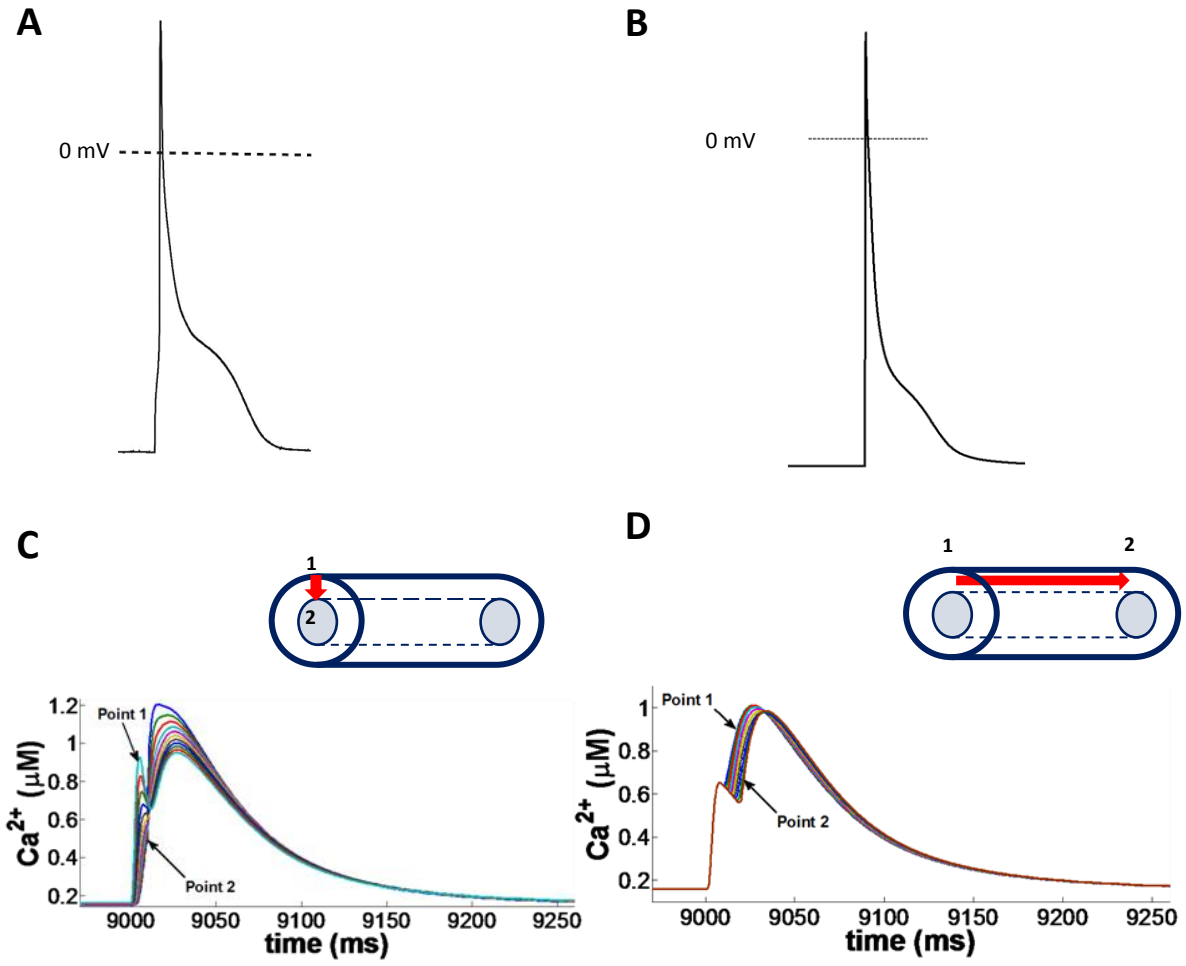

Supplemental Fig. S4. AP morphology (A) as experimentally recorded in mouse PCs by Vaidyanathan et al.,[9] (B) AP obtained from our PC model. Cytosolic Ca^{2+} transients observed in the model representing (A) diffusion of radial wavelets, and (B) longitudinal diffusion of CWW. The locations of Point 1 and Point 2 are shown on the right. The red arrow represents the component of Ca^{2+} diffusion shown.

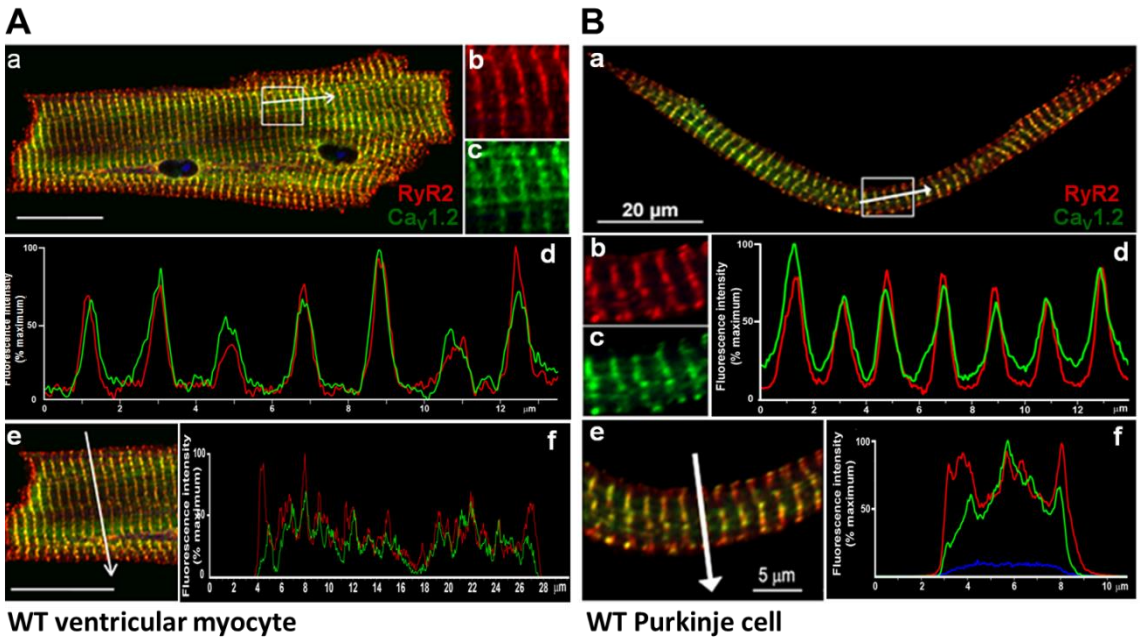

Supplemental Fig. S5. Subcellular co-localization of RyR2 and $Ca_V1.2$ is more heterogeneous in Ctrl PCs than VMs. (A) Ventricular myocyte, (B) Purkinje cell. For each Panel, subpanels (b-c) are enlarged regions of the boxed area in (a). Co-localization RyR2 and $Ca_V1.2$ is shown in (b-d) at the T-tubules and at the sarcolemma (e-f). Red, RyR2; Green $Ca_V1.2$.

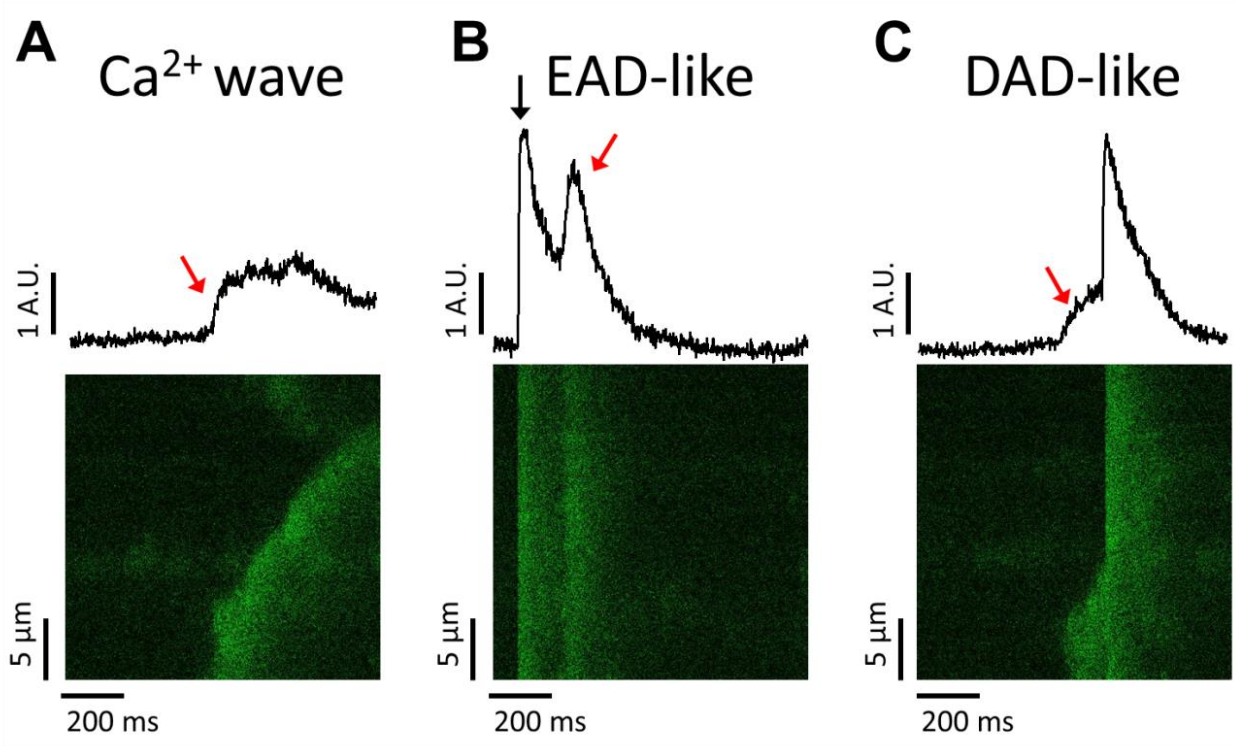

Supplement Fig. S6. Representative examples of spontaneous Ca^{2+} release in CPVT PCs perfused with 30nM Isoproterenol. Left is a diastolic Ca^{2+} wave. Middle shows an early after Ca^{2+} transient after a paced Ca^{2+} transient. Right illustrates a diastolic Ca^{2+} wave that leads to triggered activity (delayed after Ca^{2+} transient). All of these are present in both Ctrl and CPVT Purkinje cells. Black arrow marks paced beat, red arrow indicates spontaneous Ca^{2+} event.

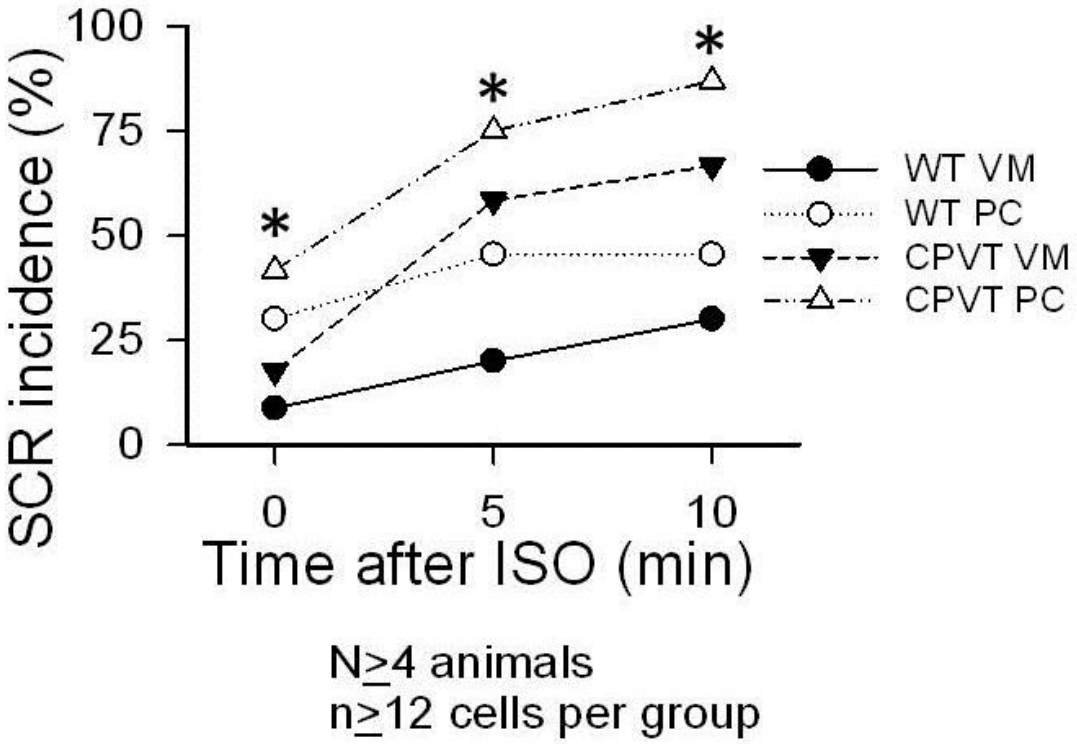

Supplement Fig. S7. Increased spontaneous Ca^{2+} release incidence in CPVT PCs. The incidence of spontaneous Ca^{2+} release increases with perfusion of 10nM isoproterenol. The incidence of SCR is higher in CPVT PCs both baseline and after ISO. *$p<0.05$ using Fisher's exact test.

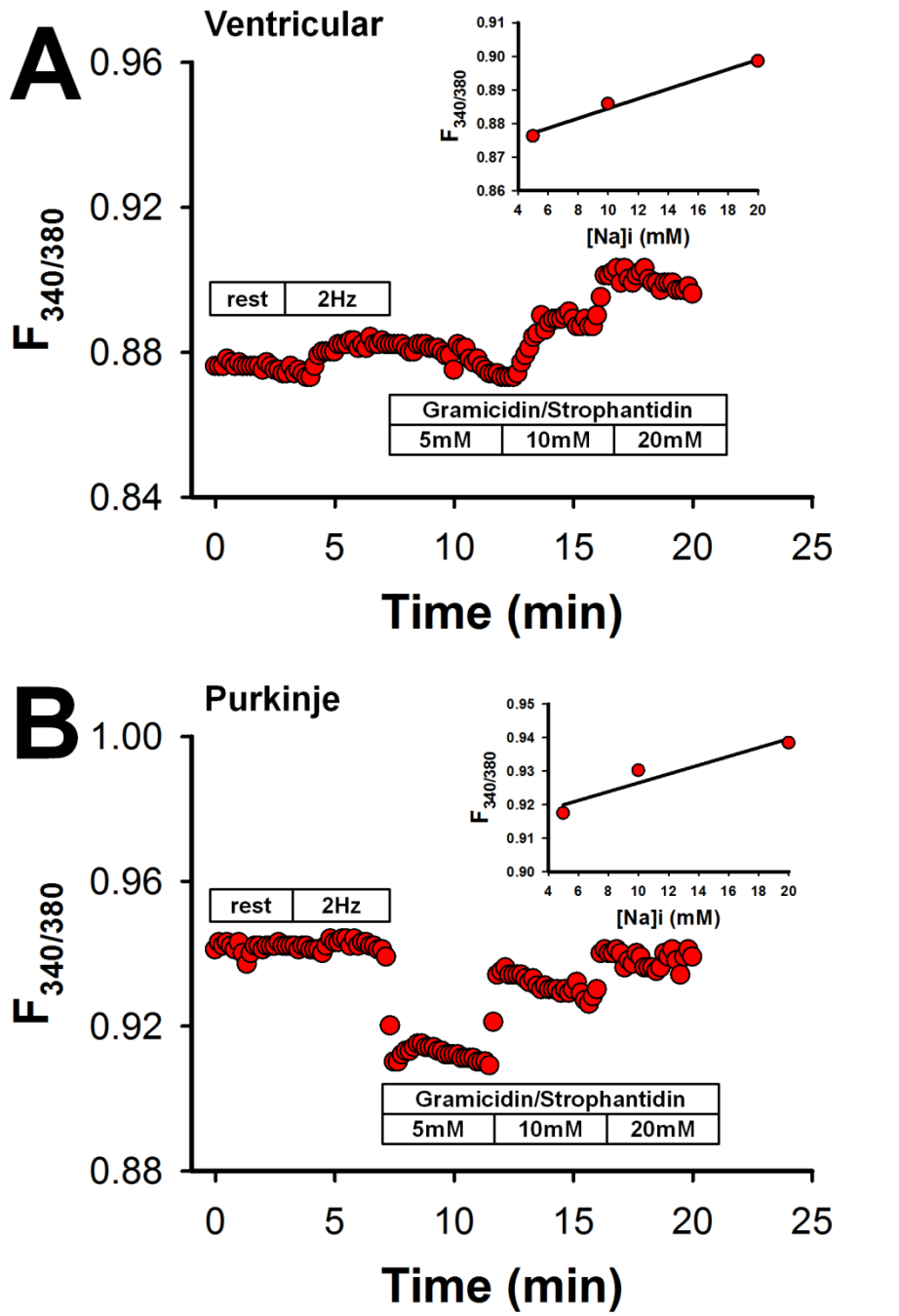

Supplement Fig. S8. Increased intracellular Na^+ in Purkinje cells compared to ventricular myocytes. Representative SFBI fluorescence recordings in (A) ventricular and (B) Purkinje cells at 37° C. Inset shows 3 point calibration performed at the end of each individual experiment after perfusion with gramicidin and strophantidin and three different increasing concentrations of Na^+.

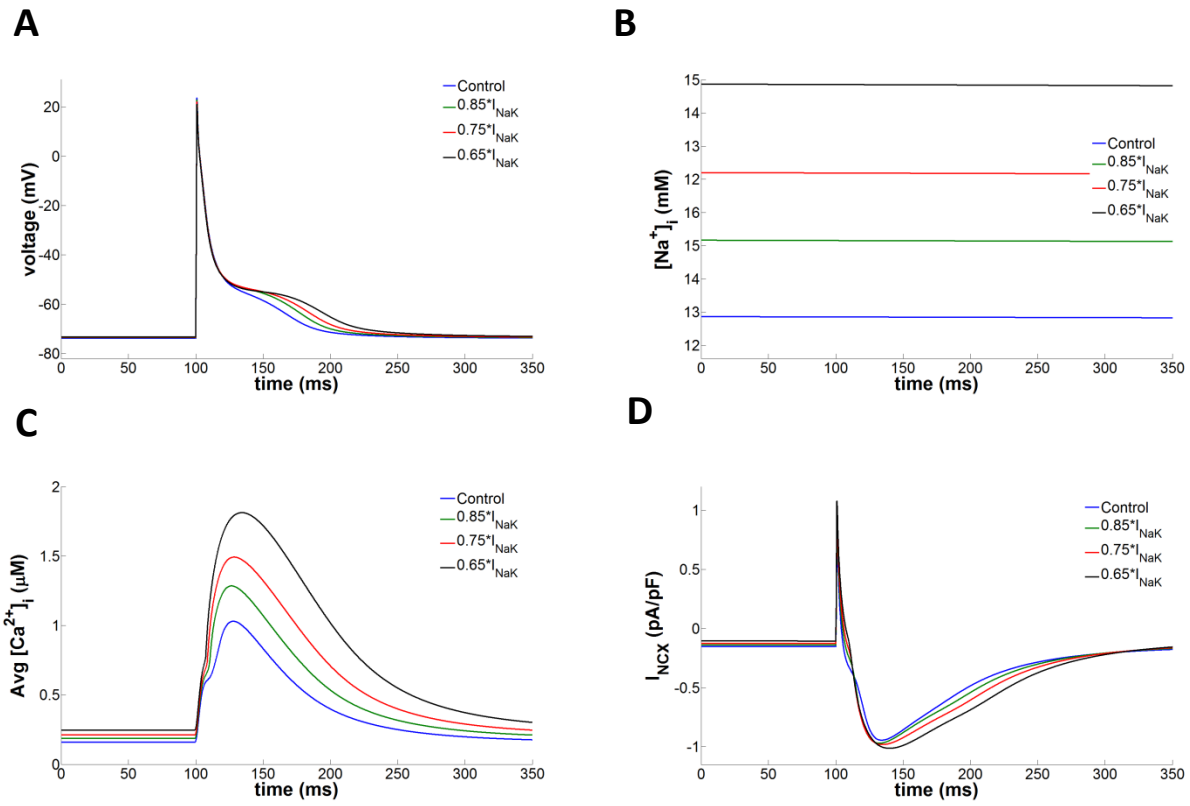

Supplemental Fig. S9. (A) Action Potentials in PC model for different scaling of I_{NaK} at 1Hz pacing. (B) Intracellular sodium concentration in PC obtained by scaling I_{NaK} at 1Hz (C) Intracellular average calcium concentrations in the model for different scaled I_{NaK} at 1Hz (D) I_{NCX} currents for different scaled I_{NaK} currents at pacing frequency of 1Hz.

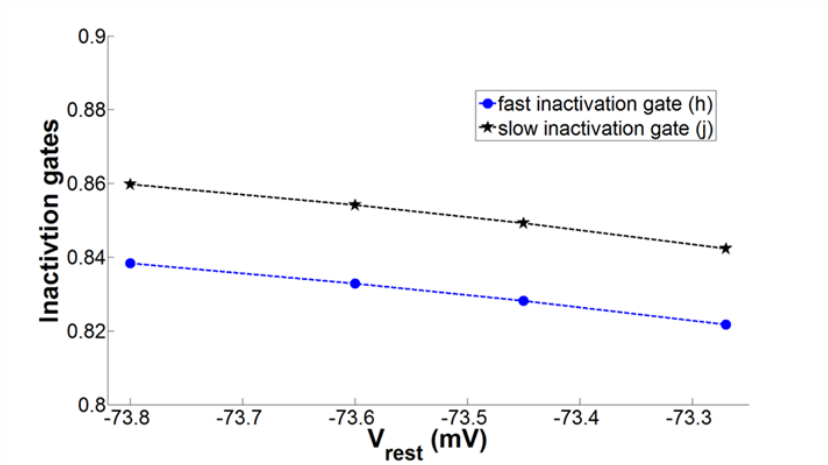

Supplemental Fig. S10. Insignificant alterations in the fast and slow inactivation gates (*h* and *j*, respectively) of I_{Na} at various resting membrane potentials resulted due to elevated levels of $[Na]_i$.

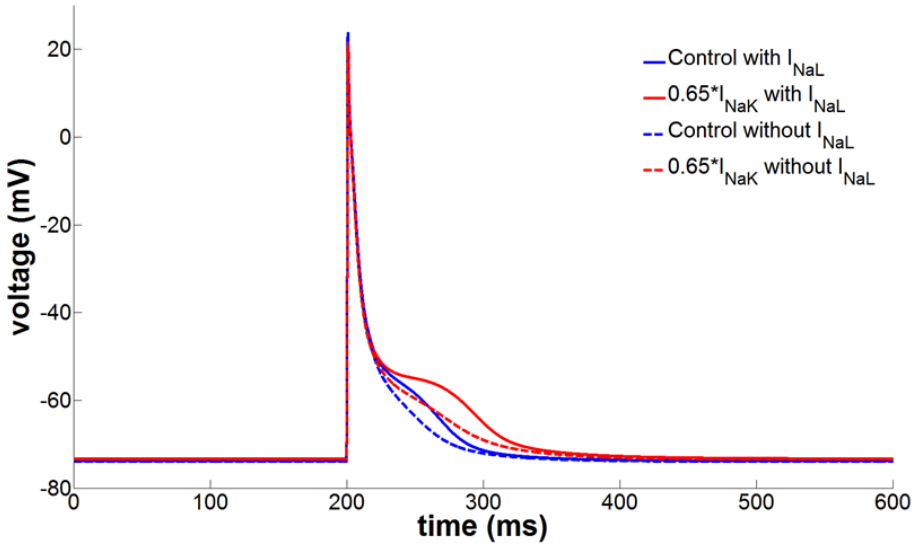

Supplemental Fig. S11. Action potentials in the PC model with I_{NaL} and without I_{NaL} for the control case and for one representative I_{NaK} value.

References:

1. Cerrone M, Colombi B, Santoro M, di Barletta MR, Scelsi M, Villani L, Napolitano C, Priori SG. Bidirectional ventricular tachycardia and fibrillation elicited in a knock-in mouse model carrier of a mutation in the cardiac ryanodine receptor. *Circ Res*. 2005;96:e77-82
2. Cerrone M, Noujaim SF, Tolkacheva EG, Talkachou A, O'Connell R, Berenfeld O, Anumonwo J, Pandit SV, Vikstrom K, Napolitano C, Priori SG, Jalife J. Arrhythmogenic mechanisms in a mouse model of catecholaminergic polymorphic ventricular tachycardia. *Circ Res*. 2007;101:1039-1048
3. Miquerol L, Meysen S, Mangoni M, Bois P, van Rijen HV, Abran P, Jongsma H, Nargeot J, Gros D. Architectural and functional asymmetry of the his-purkinje system of the murine heart. *Cardiovasc Res*. 2004;63:77-86
4. Fernandez-Velasco M, Rueda A, Rizzi N, Benitah JP, Colombi B, Napolitano C, Priori SG, Richard S, Gomez AM. Increased ca2+ sensitivity of the ryanodine receptor mutant ryr2r4496c underlies catecholaminergic polymorphic ventricular tachycardia. *Circ Res*. 2009;104:201-209, 212p following 209
5. Herron TJ, Milstein ML, Anumonwo J, Priori SG, Jalife J. Purkinje cell calcium dysregulation is the cellular mechanism that underlies catecholaminergic polymorphic ventricular tachycardia. *Heart Rhythm*. 2010;7:1122-1128
6. Lee P, Klos M, Bollensdorff C, Hou L, Ewart P, Kamp TJ, Zhang J, Bizy A, Guerrero-Serna G, Kohl P, Jalife J, Herron TJ. Simultaneous voltage and calcium mapping of genetically purified human induced pluripotent stem cell-derived cardiac myocyte monolayers. *Circ Res*. 2012;110:1556-1563
7. Noujaim SF, Pandit SV, Berenfeld O, Vikstrom K, Cerrone M, Mironov S, Zugermayr M, Lopatin AN, Jalife J. Up-regulation of the inward rectifier k+ current (i k1) in the mouse heart accelerates and stabilizes rotors. *J Physiol*. 2007;578:315-326
8. Anumonwo JM, Tallini YN, Vetter FJ, Jalife J. Action potential characteristics and arrhythmogenic properties of the cardiac conduction system of the murine heart. *Circ Res*. 2001;89:329-335
9. Vaidyanathan R, O'Connell RP, Deo M, Milstein ML, Furspan P, Herron TJ, Pandit SV, Musa H, Berenfeld O, Jalife J, Anumonwo JM. The ionic bases of the action potential in isolated mouse cardiac purkinje cell. *Heart Rhythm*. 2013;10:80-87
10. Cheng H, Song LS, Shirokova N, Gonzalez A, Lakatta EG, Rios E, Stern MD. Amplitude distribution of calcium sparks in confocal images: Theory and studies with an automatic detection method. *Biophys J*. 1999;76:606-617
11. Picht E, Zima AV, Blatter LA, Bers DM. Sparkmaster: Automated calcium spark analysis with imagej. *Am J Physiol Cell Physiol*. 2007;293:C1073-1081
12. Despa S, Islam MA, Weber CR, Pogwizd SM, Bers DM. Intracellular na(+) concentration is elevated in heart failure but na/k pump function is unchanged. *Circulation*. 2002;105:2543-2548
13. Li L, Niederer SA, Idigo W, Zhang YH, Swietach P, Casadei B, Smith NP. A mathematical model of the murine ventricular myocyte: A data-driven biophysically based approach applied to mice overexpressing the canine ncx isoform. *Am J Physiol Heart Circ Physiol*. 2010;299:H1045-1063
14. Stuyvers BD, Dun W, Matkovich S, Sorrentino V, Boyden PA, ter Keurs HE. Ca2+ sparks and waves in canine purkinje cells: A triple layered system of ca2+ activation. *Circ Res*. 2005;97:35-43
15. Crank J. *The mathematics of diffusion*. Oxford: Clarendon Press; 1975.
16. Korhonen T, Hanninen SL, Tavi P. Model of excitation-contraction coupling of rat neonatal ventricular myocytes. *Biophys J*. 2009;96:1189-1209
17. Sadiku M. *Numerical techniques in electromagnetics*. CRC Press; 2000.